

GENERAL ELECTRIC

NUCLEAR POWER
SYSTEMS DIVISION

GENERAL ELECTRIC COMPANY, 175 CURTNER AVE., SAN JOSE, CALIFORNIA 95125
MC 682, (408) 925-5722 RHB-058-80

MFN-125-80

July 14, 1980

U. S. Nuclear Regulatory Commission
Office of Nuclear Reactor Regulation
Washington, D.C. 20555

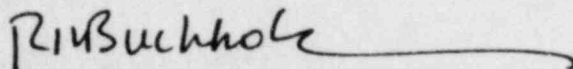
Attention: Mr. Roger J. Mattson, Director
Division of Safety Technology

Gentlemen:

SUBJECT: MARK I CONTAINMENT PROGRAM
ADDITIONAL INFORMATION ON VENT SYSTEM COMPRESSIBILITY
EFFECTS ON MARK I POOL SWELL

On April 22 and 23, 1980 representatives of the Mark I Owners Group met with the NRC staff and their consultants to discuss several subjects related to closure of the Mark I Containment Program. During these discussions, the NRC staff requested additional information regarding vent system compressibility effects on Mark I pool swell. Enclosed are ten copies of a letter report which contains the information requested by the NRC staff. This information is being provided by the General Electric Company on behalf of the Mark I Owners Group as part of the Mark I Containment Program. This report describes the additional analyses performed, discusses the results and presents conclusions relevant to the questions raised at the April meeting. The results presented in the enclosed report further support the conclusion that compressibility effects mitigate the major pool swell loads for existing Mark I operating conditions.

Very truly yours,



R. H. Buchholz, Manager
BWR Systems Licensing
Safety & Licensing Operation

RHB:rm/sem/1957

Enclosure

cc: C. I. Grimes (NRC)
K. Kniel (NRC)
L. S. Gifford (GE-Bethesda)
File: 2.10

8007210 366

RESPONSE TO NRC QUESTIONS ON NEDE-24778-P,

Vent System Compressibility-Effects on Mark I Pool Swell

W.S. Kennedy, R.C. Torok, K.C. Lee, J.M. Humphrey

Acurex Corporation
Alternate Energy Division
485 Clyde Avenue
Mountain View, California 94042

May 1980

Prepared for
General Electric Company
175 Curtner Avenue
San Jose, California 95125

1.0 Introduction/Summary

Mark I vent system compressibility was one of the subjects covered in the GE/NRC meetings held in San Jose on April 22 and 23, 1980. Specific NRC questions on the GE/Acurex pool swell model (Reference 1) were discussed, and additional analyses were requested by the NRC. This letter report describes the additional analyses, discusses their results, and presents conclusions relevant to the questions raised at the April meetings.

The additional compressibility analyses discussed in this response provide further insight into the effects of vent compressibility on pool swell response. Specifically, the falling vent exit (bubble) pressure history following peak download is primarily responsible for the compressible mass defect at full scale which mitigates the upload. Compressibility effects arising out of the vent inlet conditions (e.g., drywell pressure ramp) do not have a significant effect on either mass defect or upload mitigation.

The compressible mass defect at peak upload has been quantified at approximately 7% using either common scaled bubble pressure histories at quarter and full scale or using the pool model to generate different bubble pressure histories. A simple model has been used to show that a 7% mass defect is consistent with a 20% upload reduction which agrees with the magnitude of upload mitigation reported in Reference 1. These results further support the conclusions presented in Reference 1.

2.0 Background

During 1979 P.L. Chambré, working under contract to EPRI, reported that vent system compressibility effects which were not being modeled in subscale pool swell tests could affect the pool swell transient. In response to this concern a one dimensional compressible vent system model was developed. This vent system model was coupled to a bubble/pool model to quantitatively investigate vent system compressibility effects on Mark I pool swell loads. The results presented to the NRC in October 1979 and documented in Reference 1 showed the compressibility effects mitigated pool swell loads over the range of Mark I conditions and upload in particular was mitigated by about 15%. The investigation also showed that conservatism in the QSTF (Quarter Scale Test Facility) test specification typically added another 4 to 6% margin to the loads.

As part of the pool swell load investigation reported in Reference 1 the GE/Acurex model was evaluated under a variety of initial conditions for the purposes of verification, calibration, space and time step closure and phenomena understanding. Based on this work it was determined that compressibility effects were primarily the result of communication delays within the vent system due to the acoustic propagation times.

Two principal manifestations of communication delays were observed and reported in Reference 1. Prior to vent clearing the vent system exhibits a classic closed pipe response to the drywell pressure ramp. This effect causes the download to be influenced by the phasing of the acoustic wave at the time of vent clearing.

Changes in exit condition, specifically reductions in exit pressure during bubble expansion, are followed by a delayed response in exit mass flow. This delay is due to the time required for an acoustic signal to communicate with the drywell or significant capacitances within the vent system. This phenomenon which was called "compressible mass decrement effect" in Reference 1 is primarily responsible for the reduction in upload predicted with vent compressibility effects properly included.

As an aid to phenomena understanding (specifically upload mitigation) the vent model was run decoupled from the pool model for two study cases A and B and the results were reported in Reference 1.

Simplified boundary conditions which approximated the pressure histories at the entrance and exit were separately applied to full scale and quarter scale vent models and the exit mass rates were compared. This approach eliminated concerns about scaling the bubble model and showed that more mass flows from the QSTF vent than from a full scale vent (scaled to quarter scale) under the simplified boundary condition.

The vent models are shown in Figures 1 and 2. The full scale vent model has constant area but included all the estimated full scale losses due to entrance, friction, turning, branch and dump. The quarter scale model scaled all lengths, and areas, assumed the same flow losses as full scale caused by entrance, friction, turning, branch and dump, and concentrated the additional $F1/D$ required by Moody scaling in two locations approximately

where QSTF orifices were located. An isentropic entrance convergence section was included in both models so that entrance stagnation conditions could be conveniently specified. The inclusion of the dump loss in scaling the full scale losses to quarter scale is explained in Appendix A.

Boundary conditions from cases A and B are shown in Figure 3. In case A, a ramp stagnation pressure increase with $\dot{P} = \text{constant}$ was imposed at the entrance and the exit static pressure was held constant at the initial pressure. For case B the exit static pressure was stepped down, and the entrance stagnation pressure was held at the initial pressure. The use of a ramp stagnation pressure at the vent entrance simulates the drywell pressure history, and hence no drywell was needed in the model. A sudden drop at the exit simulates the demand placed on the vent due to bubble expansion.

Results from these cases were reported in Reference 1 and are repeated in Figures 4 and 5. Case B, which simulates the vent system response to bubble expansion, shows that the full scale mass flow takes longer to reach equilibrium and exhibits a clear mass flow deficiency relative to quarter scale. Note that the scaled initial flow rate at quarter scale is twice the full scale value. This occurs because for equal pressure ratios at the same temperature both scales have the same initial exit velocity and as a result the initial scaled quarter scale flow rate exceeds the full scale value by $(\text{scale factor})^{-1/2} = 2$. Case A, which simulates the response of an open vent system to the drywell pressure ramp, shows a clear time delay for the initiation of flow at full scale. In addition to the time delay, which is the dominant effect, there is an apparent mass defect due to compressibility. However a comparison of Figures 4 and 5 shows that even accounting for the scale difference, the step change in exit pressure was clearly more effective at creating a compressible mass defect than the ramp inlet pressure.

3.0 Additional Analyses

A specific NRC request from the April 22 and 23 meetings in San Jose was to recalculate the mass defect due to compressibility as shown in Figure 6-2 of Reference 1 using a more prototypical vent configuration and boundary condition. In addition to this calculation (Case 2), several other analyses are included as outlined below:

- 1) The Reference 1 mass defect analyses were reviewed; this report includes a

detailed description of the vent model and boundary conditions used to generate Figures 6-2 and 6-3 of Reference 1.

- 2) The Reference 1 analyses (Cases A and B) were rerun using a more prototypical vent system configuration. (Cases 1 and 3)
- 3) The Case A analysis from Reference 1 was repeated using a more prototypical vent system and constant drywell entrance mass flow boundary condition rather than the vent entrance pressure ramp used in Reference 1. (Case 2)
- 4) To quantify compressible mass defect with prototypical conditions at both vent system boundaries, comparisons of quarter scale and full scale vent exit flows were made using a constant \dot{m} boundary at the drywell entrance and a prototypical bubble pressure history imposed at the vent exit. (Case 4)
- 5) Compressible mass defect in a Reference 1 type pool swell analysis was quantified through comparison of QSTF "perfect" and full scale analyses. (Case 5)
- 6) A simplified pool swell analysis was performed to relate mass defect magnitude to upload reduction magnitude.

Test cases 1-3 predicted compressible mass defects ranging from 7 to 11.4%. Scaled mass flow in a sample quarter scale pool swell transient was found to be about 7% greater than the full scale value for the same transient. The resulting peak uploads differed by about 18%. The simplified pool swell analysis, described in section 3.2, confirmed this result, predicting that a 7% mass defect would cause a 20% upload reduction.

The basic explanation of the reduced uploads under compressible flow remains that Mach number was not scaled in the incompressible Moody Scaling Laws and this results in excess scaled mass flow from a duct under transient conditions of a sudden demand at the duct exit.

3.1 Nodal Configuration and Boundary Condition

The requested additional analyses used a more prototypical nodal system shown in Figures 6, 7, 7A. Vent area changes and a drywell were included. The "quarter scale" vent models were run at a scale factor of .2801 since the full scale nodal system was for Monticello and $\lambda = .2801$ was the QSTF scale factor for Monticello. The additional F1/D required for Moody scaling was added to the subscale model in two fashions: a) by directly ratioing each nodal loss (distributed); b) by adding the additional resistance in two nodes approximately where the QSTF orifices were placed (lumped). Note that the additional F1/D when added at an area different than the exit (reference) area was ratioed by $\left(\frac{A_{local}}{A_{exit}}\right)^2$. Again, the dump loss was included in the scaling as discussed in Appendix A.

Three sets of boundary conditions were used to reexamine the Reference 1 test cases: Case 1 - pressure ramp in drywell, constant exit static pressure; Case 2 - constant drywell pressure, sudden drop in exit pressure; Case 3 - constant mass flow into drywell. Cases 1 and 2 correspond to Cases A and B of Reference 1 with the new nodalization. Case 3 was run in response to the NRC request of April 23.

Two more analyses, Cases 4 and 5, were run to quantify compressible mass defect in a pool swell transient. Case 4 was designed to isolate compressible vent flow effects from bubble model effects while keeping all the vent system boundary conditions as prototypical as possible. Case 5 evaluated compressible mass defect in a typical pool swell analysis including the bubble model.

The case 4 analysis had two parts. First, a subscale pool swell transient was run using the Figure 7A (lumped losses) nodalization to generate a "typical" scaled bubble pressure history. Initial conditions were those of a quarter scale zero ΔP transient. Constant mass flowrate into the drywell was used as the inlet boundary condition. Next, a full scale (Figure 6 nodalization) transient was run in which the vent clearing model was used almost

up to the time of clearing; thereafter, the scaled up bubble pressure from the subscale run was imposed at the vent exit. Case 4A repeated the Case 4 exercise using the QSTF "Perfect" (Figure 8) and full scale (Figure 6) nodalizations. Case 5 used the QSTF "Perfect" and full scale nodalizations in pool swell runs (with the bubble model) to quantify the compressible mass defect in a Reference 1 type analysis. Initial and boundary mass conditions were identical to those used in the Case 4 zero ΔP transients. Time steps selected were $\Delta t = .00025$ sec subscale and $\Delta t = .0005$ sec full scale based on the time step study reported at the April 22-23 meeting.

3.2 Analysis Results

Results for Case 1, a 60 psi/sec full scale ramp and Case 3, a constant mass rate = 386.92 lbm/sec into the drywell, are shown in Figures 9 through 12. Drywell pressure histories for Case 3 are shown in Figures 13 and 14. Note that the QSTF type resistance placement resulted in better simulation of the drywell pressure transients than the ratioed F1/D configuration due to a slightly larger effective drywell capacitance for the distributed case. Results for Case 3 using the QSTF type F1/D distribution (Figures 12 and 14) are considered more representative since similar drywell histories resulted.

A small mass defect is observable in Case 1 and no net effect can be seen in Case 3. These results, which indicate essentially no net mass defect for the pressure ramp type boundary condition, are in conflict with the previously reported results shown in Figure 4. Explanation for this difference probably lie in some combination of the following considerations: 1) more prototypical nodal system; 2) scale factor = .28 rather than .25; and 3) "qualitative" nature of the shaded region in Figure 4.

Results for Case 2, the sudden pressure drop at the exit, are shown in Figures 15 through 18. In general the mass defect due to compressibility was not altered by the new nodal system. The Reference 1 mass flow curves (Figure 5) have less fine structure than the new (Figures 15 and 16) results. This is due to the more complicated arrangement of losses and capacitances in the new (prototypical) nodalization. Rearrangement of major system losses relative to capacitances results in the differences between the curves in Figures 5, 15, and 16. The small steady state flow rate difference in Figure 16 between full scale and scaled quarter scale (slightly higher) arises from scaling vent system F1/D by $1/\lambda$. This approach

results in slightly conservative subscale vent system flow rates.

At the April 23 meeting a question was raised concerning the appropriate way to treat the dump loss when scaling total vent system resistance $F1/D$. The analysis in Appendix A confirms that the dump loss should be included when scaling the $F1/D$ (which was the approach taken for the QSTF tests),

Drywell pressure and vent exit pressures from Case 4 (bubble pressure history at vent exit) are compared in Figures 19 and 20. Because the switch from calculated exit pressure to imposed exit pressure in the full scale run occurs before clearing, and vent exit conditions at the switch time are not identical in the two runs, the two systems clear at slightly different pressures and the exit pressure curves do not exactly coincide.

Mass flowrate and integrated mass comparisons are based on flow at the initial waterslug surface. The curves were offset in time until the integrated masses were the same at the time of clearing (at clearing the integrated mass in each case must be exactly that required to displace the waterslug). The precise timeshift required was determined using integrated mass values printed at each timestep in the computer runs. Mass flowrates and integrated mass comparisons are shown in Figures 21 and 22. In Case 4 the required timeshift was less than .001 second. The total mass defect at the time of peak upload (.486 sec. from the subscale run with the bubble model) was 7.7%.

In Case 4A, the repeat of Case 4 using the QSTF "Perfect" subscale model, the slightly different distribution of losses and capacitances in QSTF "Perfect" resulted in better drywell pressure agreement between subscale and full scale (Figure 23). Vent exit pressures and integrated mass flow comparisons are shown in Figures 24 and 25. In Case 4A the total mass defect at the time of peak upload (.484 sec) was 11.4%.

Results for Case 5, the QSTF "Perfect" vs full scale pool swell transients are shown in Figures 26 through 29. Drywell pressure histories (Figure 26) showed excellent agreement; bubble pressure (Figure 27) deviated as in the Reference 1 analyses. Mass flow comparisons (Figure 28 and 29) include a .003 sec timeshift to make the subscale and full scale clearing times the same. Peak upload occurs at .484 sec in subscale and .491 sec in full scale. The total mass defect at peak upload was 7.1%.

4.0 Discussion

Study cases A and B of Reference 1 demonstrated that compressible effects can modify the scaled mass flow transients in a simplified vent system subjected to simplified boundary conditions, the flow being driven in one case by a ramped inlet pressure and in another by a sudden pressure drop at the exit. Cases 1, 2, and 3 of the current study were intended to quantify the Reference 1 result using a prototypical vent system.

The sudden exit pressure drop case (Case 2) produced a significant mass defect between full scale and quarter scale, thereby confirming the results presented in Reference 1. However the ramp entrance pressure case (Case 1) and the constant \dot{m} into the drywell case (Case 3) when appropriately time shifted showed only small and probably insignificant flow rate differences due to compressibility.

These results led to the further understanding that compressibility effects due to vent system entrance conditions at the initiation of a LOCA acted primarily to time shift the event. The compressible mass defect responsible for pool swell mitigation is almost entirely due to the additional time required for a compressible system to respond to the mass flow requirements at the vent exit. This effect is observable even before vent clearing (i.e. the exit pressure oscillates about the inlet pressure ramp for the closed pipe response, but at zero ΔP the exit pressure never crosses the drywell pressure due to the volumetric increase in the downcomers caused by the accelerating waterslug) and is accentuated following vent clearing.

The vent exit (bubble) pressure transient is the primary factor determining the magnitude of the compressible mass defect, and the degree of upload mitigation. Thus additional analyses reported in this response were directed at quantifying the mass defect, confirming that the calculated upload mitigation was reasonable and evaluating the sensitivity of this effect on the bubble pressure history. Cases 4, 4A and 5 show that variations in the bubble pressure histories and in the models consistently produce mass decrements of 7% to 11%. Removing the bubble model and using the same bubble pressure history for full scale and quarter scale results in a high (more optimistic) value of mass defect. Including the bubble model gives a more conservative and probably more realistic value because the bubble model provides a feedback mechanism whereby the lower compressible flow rate results in a lower bubble pressure which acts to increase the flow rate and reduce the magnitude of the mass defect.

A simplified model was developed to estimate the effect of mass defect on peak upload and thereby check the computer results presented in Reference 1. Those calculations predicted an upload reduction of 13% to 18% over the range of Mark 1 water legs. The mass defect calculated for this response at zero ΔP for Cases 4 and 5 ranged from 7.1% to 11.4%. The following analysis shows that a mass defect of 7% could be expected to reduce peak upload by roughly 20%.

Consider the simplified slab bubble model in Figure A.

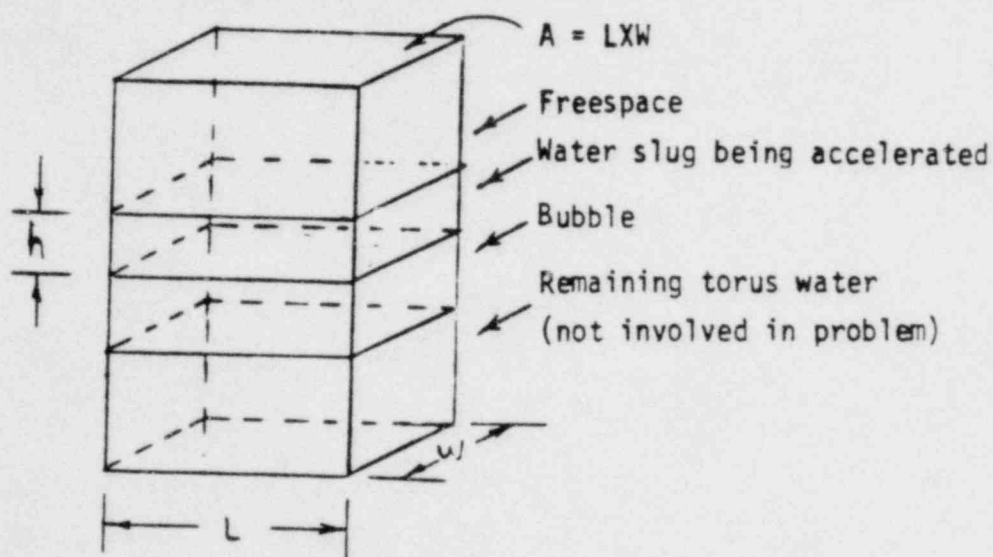


FIGURE A. SLAB BUBBLE MODEL

$$\text{Upload} = (P_{fs} - P_B + \rho gh) A \quad (1)$$

- Where
- P_{fs} = Freespace pressure
 - P_B = Bubble pressure
 - ρ = Water density
 - g = gravitational constant
 - h = Thickness of water slug
 - A = Effective area

The model calculates freespace pressure and volume using:

$$P_{fs} V_{fs}^{\gamma} = \text{constant}, \quad (2)$$

$$\text{and } V_{fs} = V_{fs \text{ initial}} - V_B \quad (3)$$

where V_{fs} = Freespace volume

V_B = bubble volume

Using quarter scale values from Case 5, $\gamma = 1.2$ (Ref. 1)

$$V_{fs \text{ initial}} = 44.24 \text{ ft}^3$$

$$P_{fs \text{ initial}} = 4.08 \text{ psia}$$

$$PV^{\gamma} = 385.16$$

At peak upload, $V_B = 18.0 \text{ ft}^3$, $P_B = 5.9 \text{ psia}$ (These are approximate values taken from the Case 5 analysis. They need not be exact for the purposes of this analysis.)

$$P_{fs} = \frac{385.16}{(44.24-18)^{1.2}} = 7.636 \text{ psia}$$

If bubble mass were decreased by 7% without changing pressure (assuming the same bubble pressure and temperature history)

$$P_{fs} = \frac{385.16}{[44.24-18(.93)]^{1.2}} = 7.218 \text{ psia}$$

Assuming an initial hydrostatic head of .4 psia at the vent exit, and using the upload expression given in equation 1, the ratio of peak uploads for the two cases is:

$$\frac{F'}{F} = \frac{7.218 - 5.9 + .4}{7.636 - 5.9 + .4} = .804 \quad (4)$$

With the assumptions outlined above, a 7% mass defect gives a 20% upload reduction. This occurs primarily because the bubble pressure datum term $(-5.9+.4)$ in the force calculation reduces both the numerator and denominator in the load ratio expression (eqtn. 4), making the ratio more sensitive to small changes in freespace pressure.

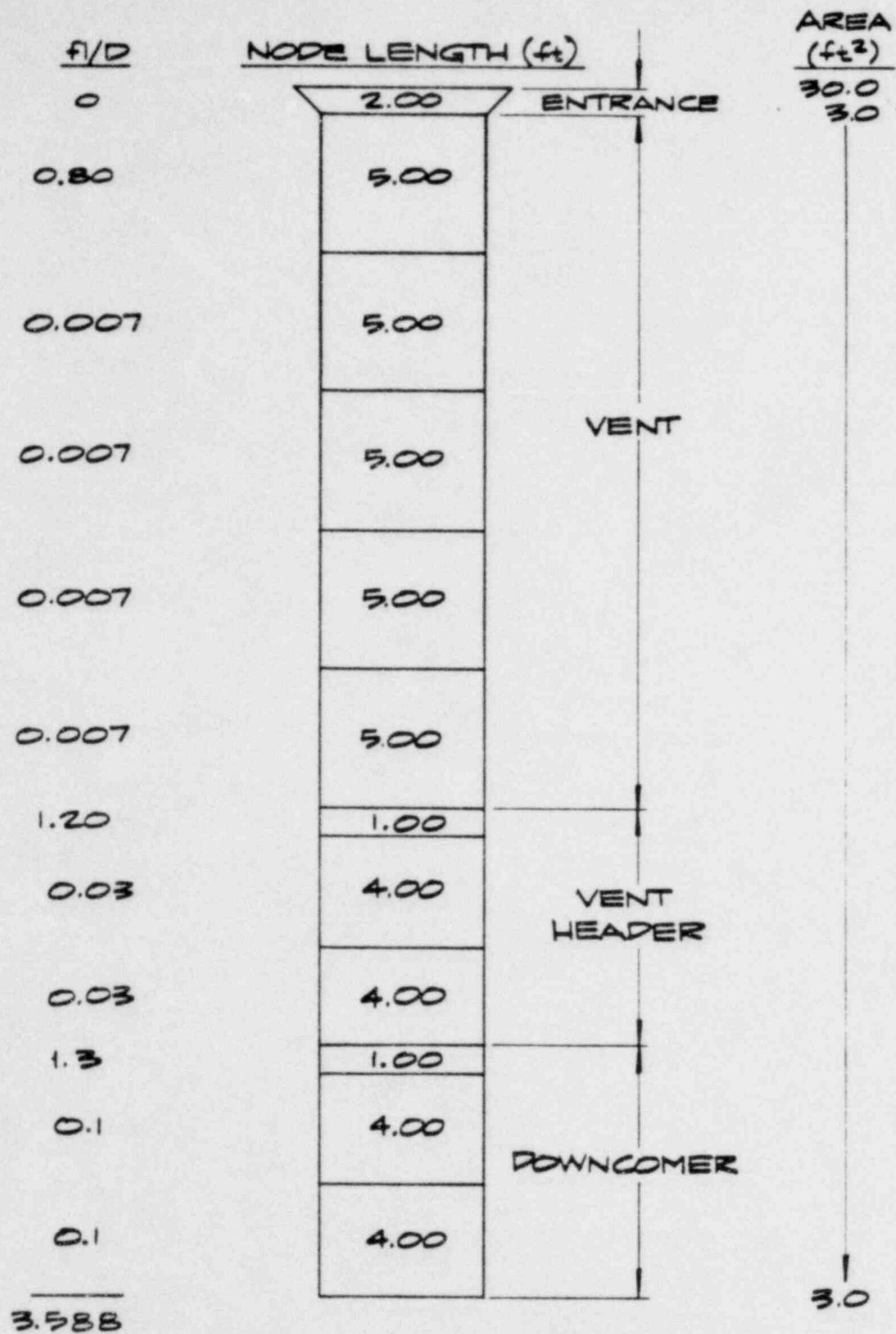
Actual pool swell transients are more complicated in that the bubble pressure histories at subscale and full scale differ due to the effects of compressibility. However, in comparing bubble pressure histories reported in Reference 1 (Figures 7.3, 7.4, and 7.5), the full scale trace appears to oscillate about the subscale trace and the values are quite close to each other at the time of peak upload. Hence the simple analysis alone, based on equal bubble pressure histories, comes close in predicting the correct state points of freespace pressure and upload ratios. Thus, the 7.1-11.4% mass defects predicted in Cases 4 and 5 are consistent with the 13-18% upload reductions reported in Reference 1.

5.0 Conclusions

1. The compressible mass defect which acts to mitigate pool swell loads is primarily due to the delayed full scale response to vent exit conditions.
2. The compressible system response to a ramp pressure entrance condition is primarily a time shift in the initiation of the event without any significant mass defect.
3. Mass defects for several prototypical exit conditions ranged from 7.1% to 11.4%.
4. Based on a simplified pool swell analysis, assuming similar bubble pressure histories, a 7% mass defect leads to a 20% upload reduction which is consistent with results reported in Reference 1.

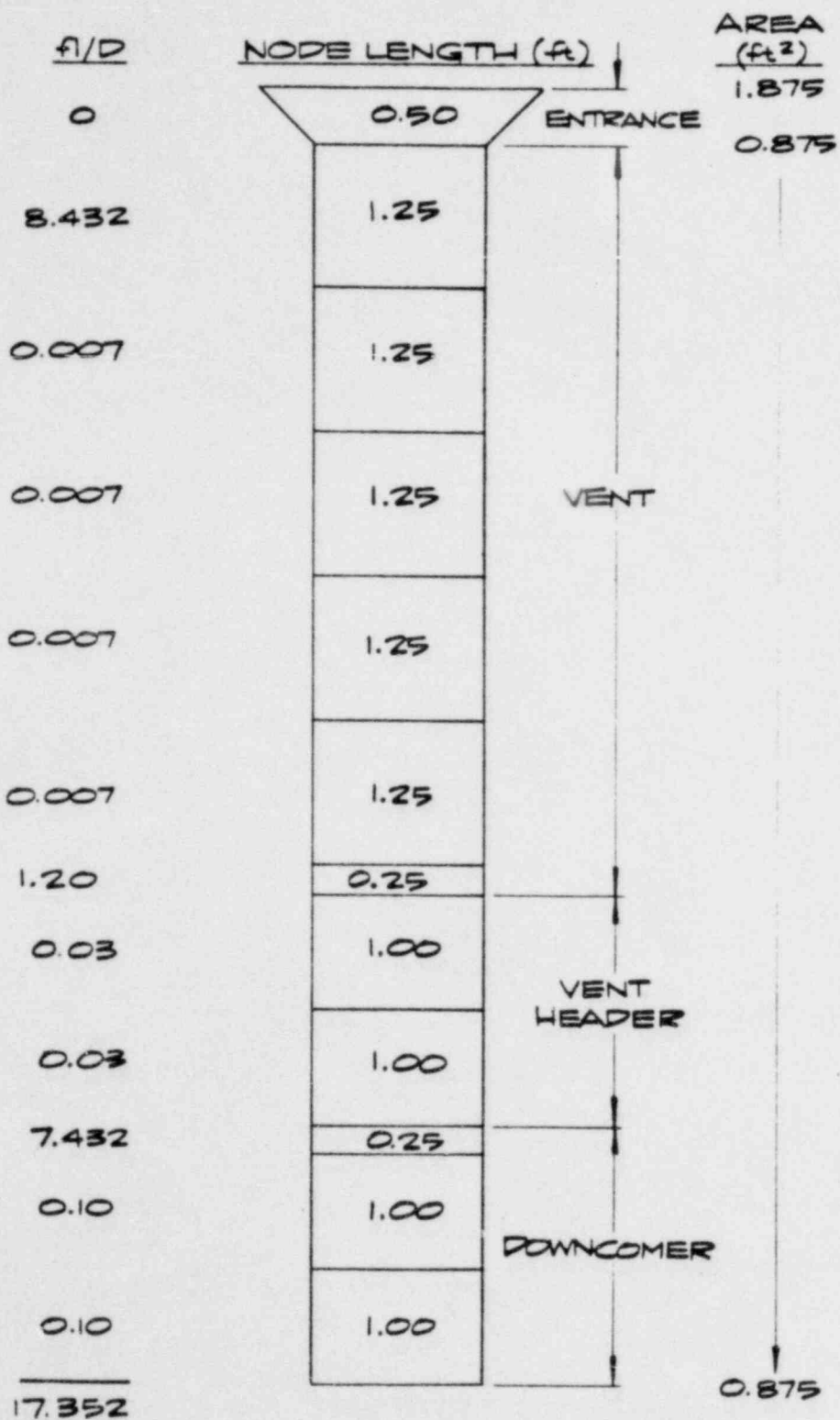
6.0 References

- 1) NEDE-24778-P, "Vent System Compressibility - Effects on Mark I Pool Swell," January 1980.
- 2) Moody, F.J., "A Systematic Procedure for Scale-Modeling Unsteady Thermo-Fluid Systems," General Electric Co. NEDO-25210.



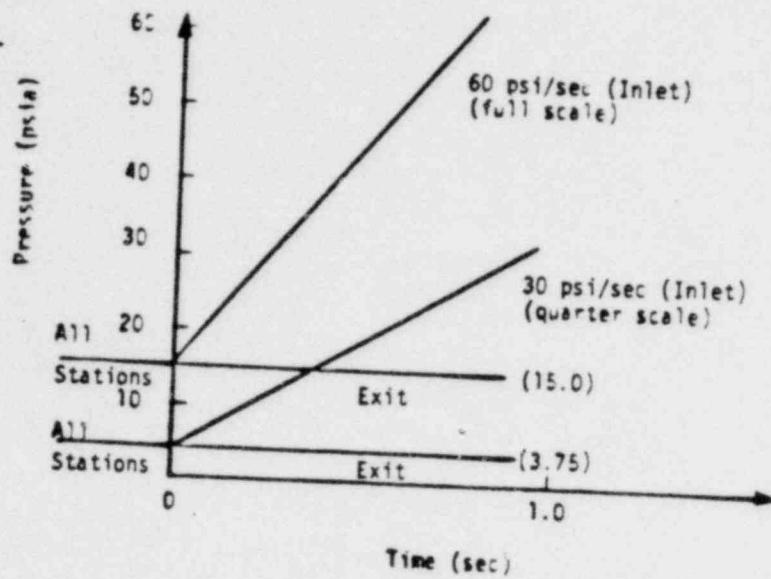
TOTAL VENT $f/D = 3.588 + 1.0 = 4.588$
(DUMP)

Figure 1. Full Scale Vent (from Reference 1)



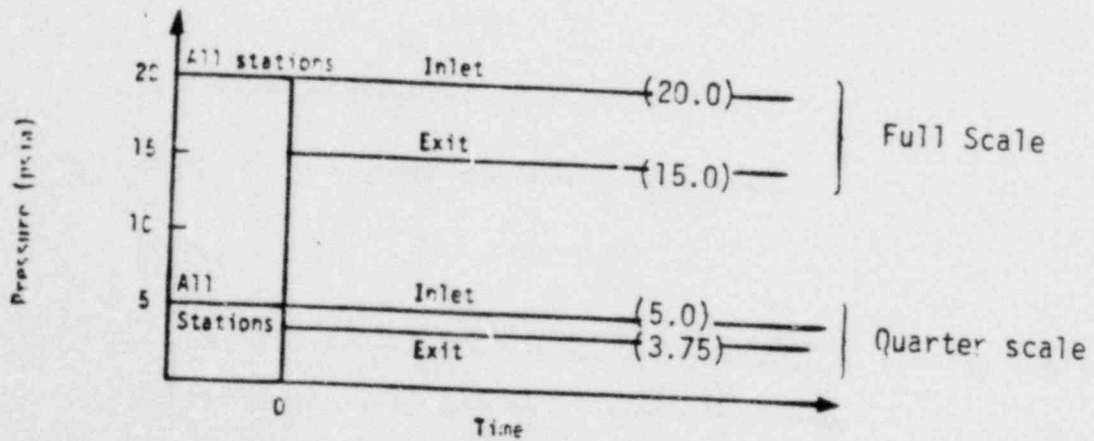
TOTAL VENT $f/D = 17.352 + 1.0_{(DUMP)} = 18.352$
 $= 4 \times (\text{FULL SCALE } f/D)$

Figure 2. Quarter Scale Vent (from Reference 1)



Test Case A. Ramp pressure increase at entrance.

Simplified Vent Model
Initial and Boundary Conditions



Test Case B. Step change in exit pressure.

Figure 3. Compressibility study cases.

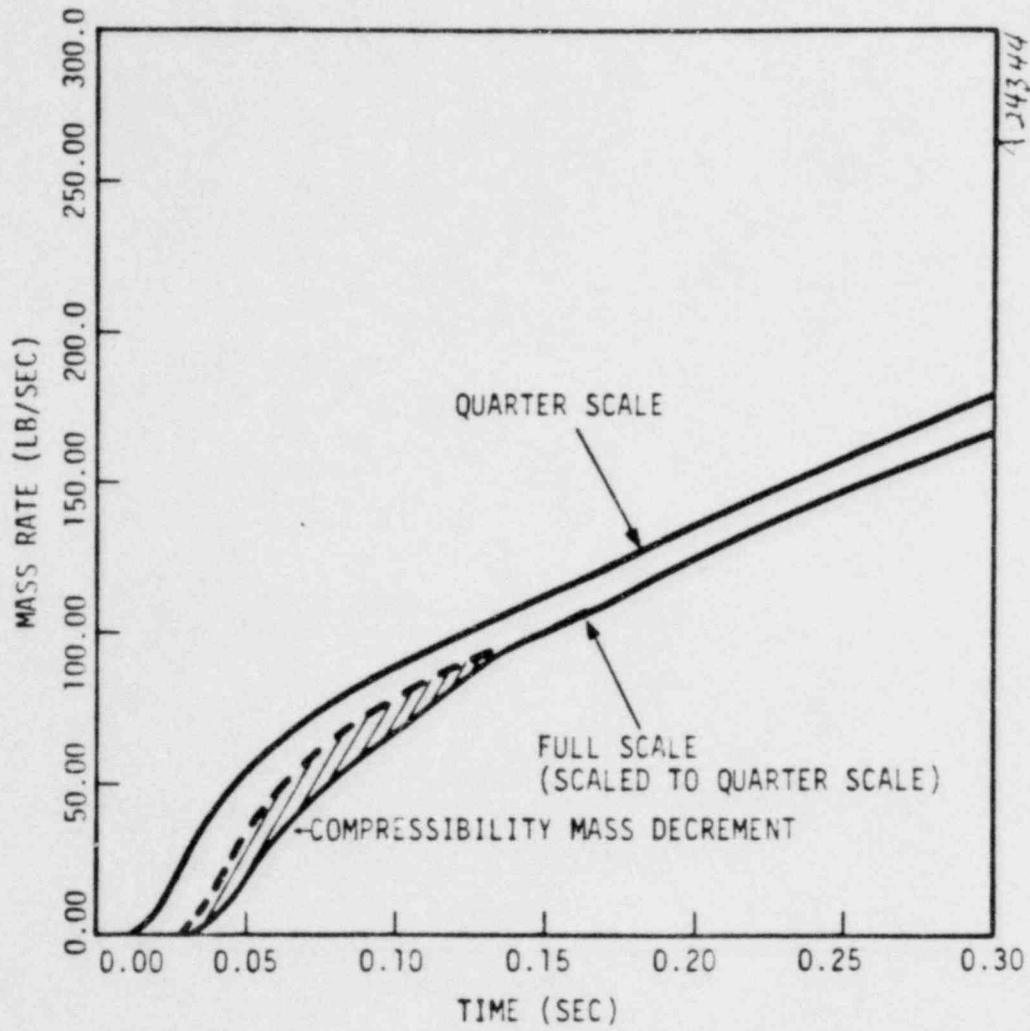


Figure 4. Compressibility study case A.

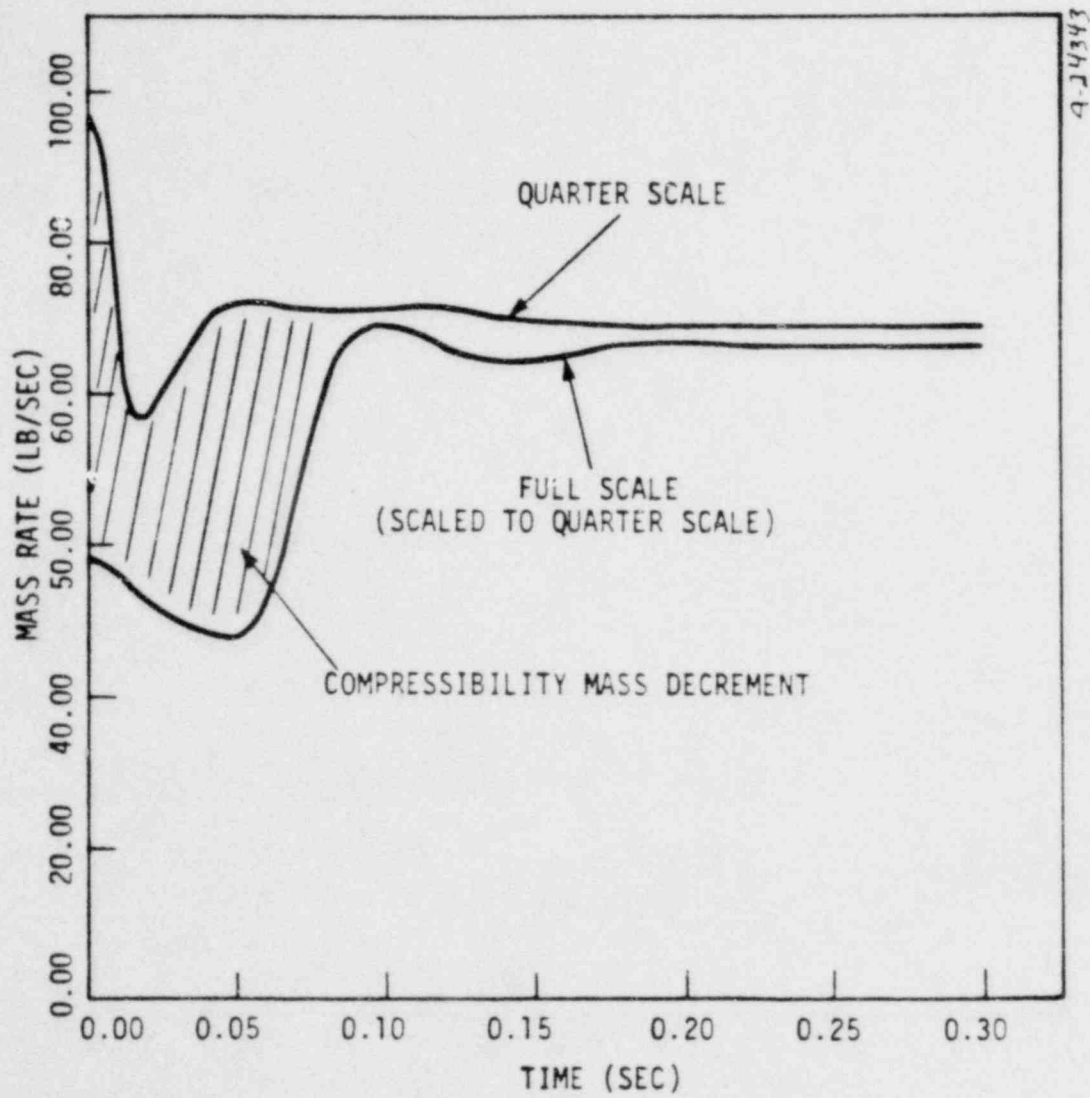


Figure 5. Compressibility study case B.

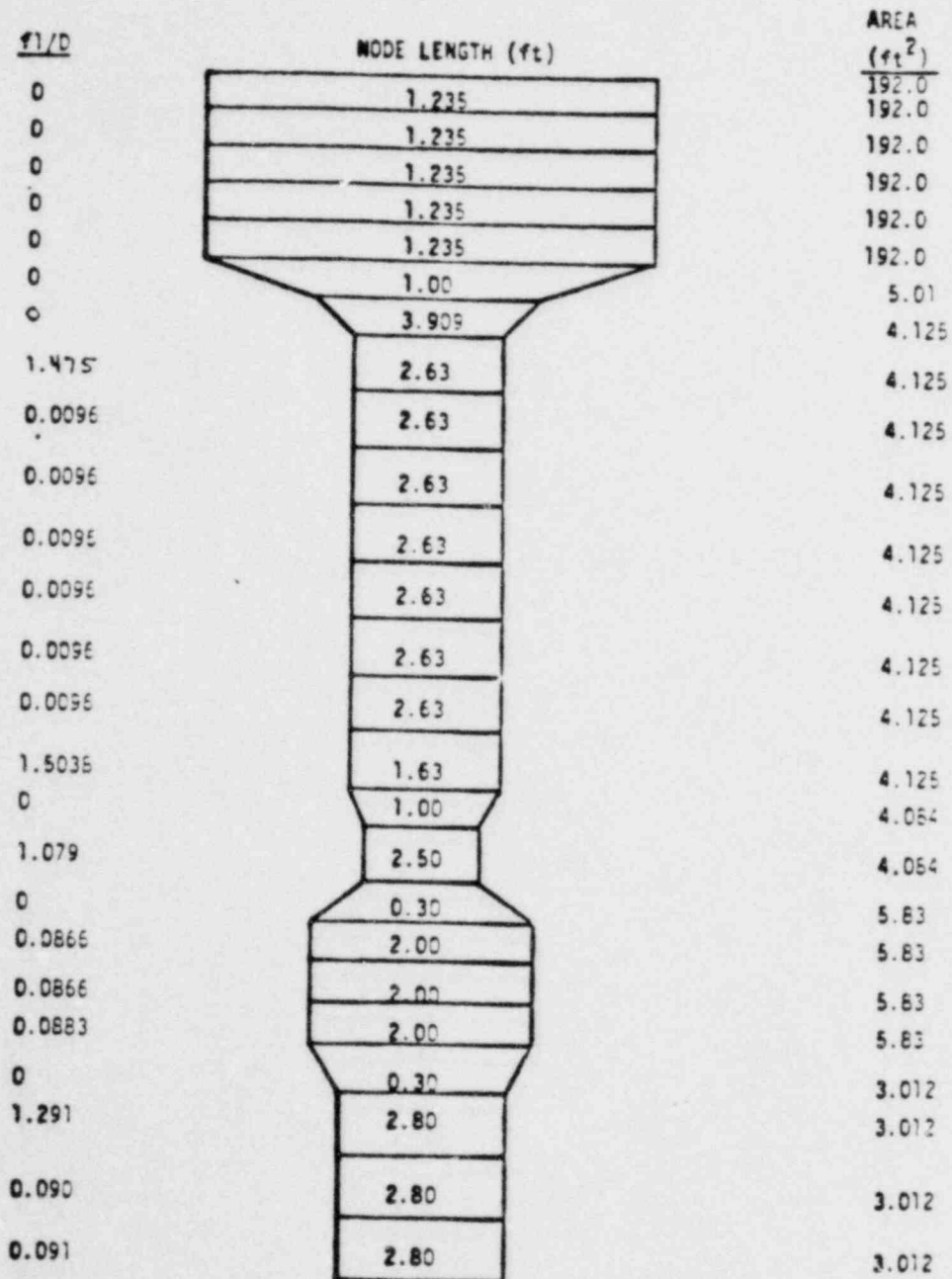


Figure 6. Full scale vent system -- 26-node configuration.

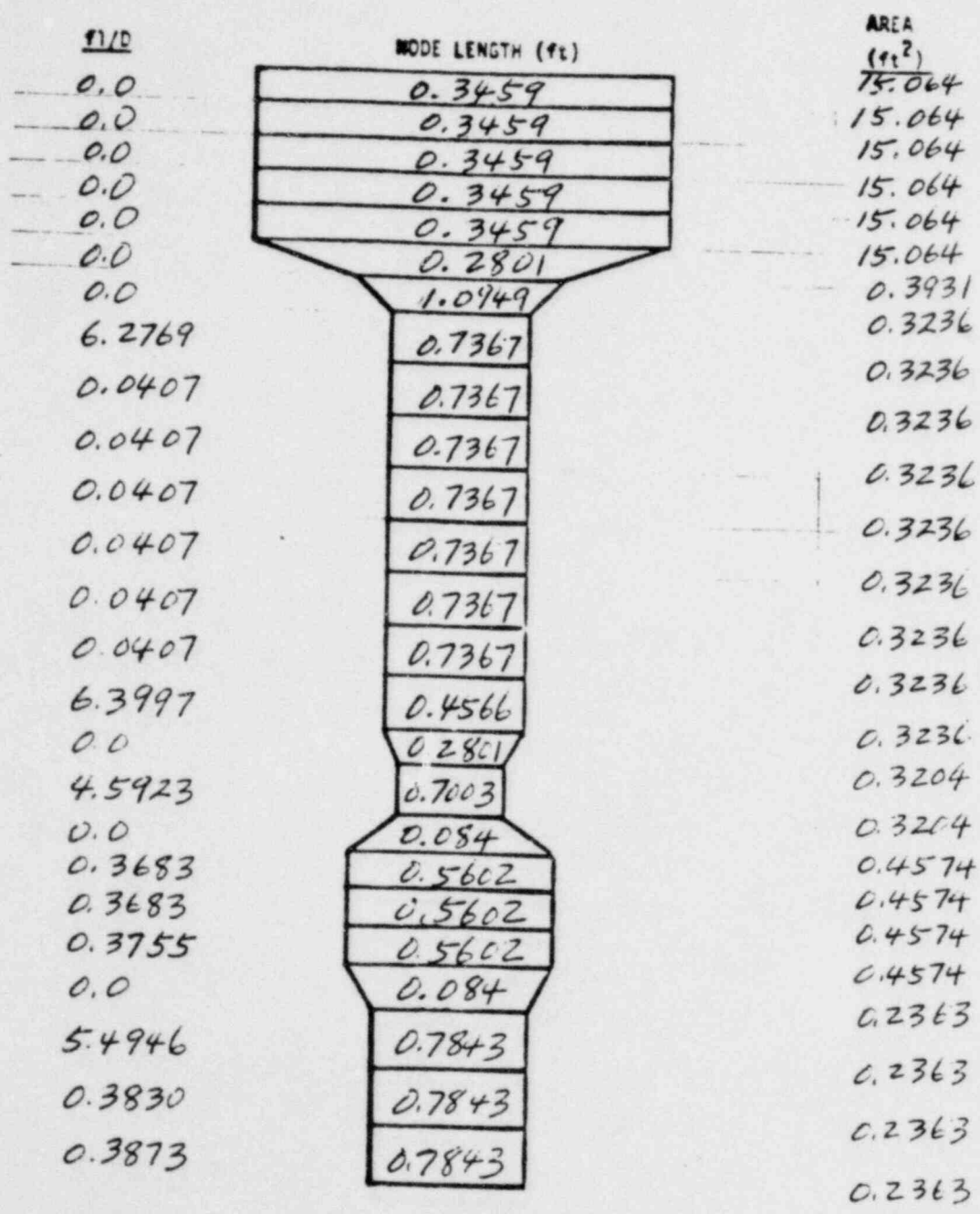


Figure 7. Subscale Vent System with Distributed F1/D

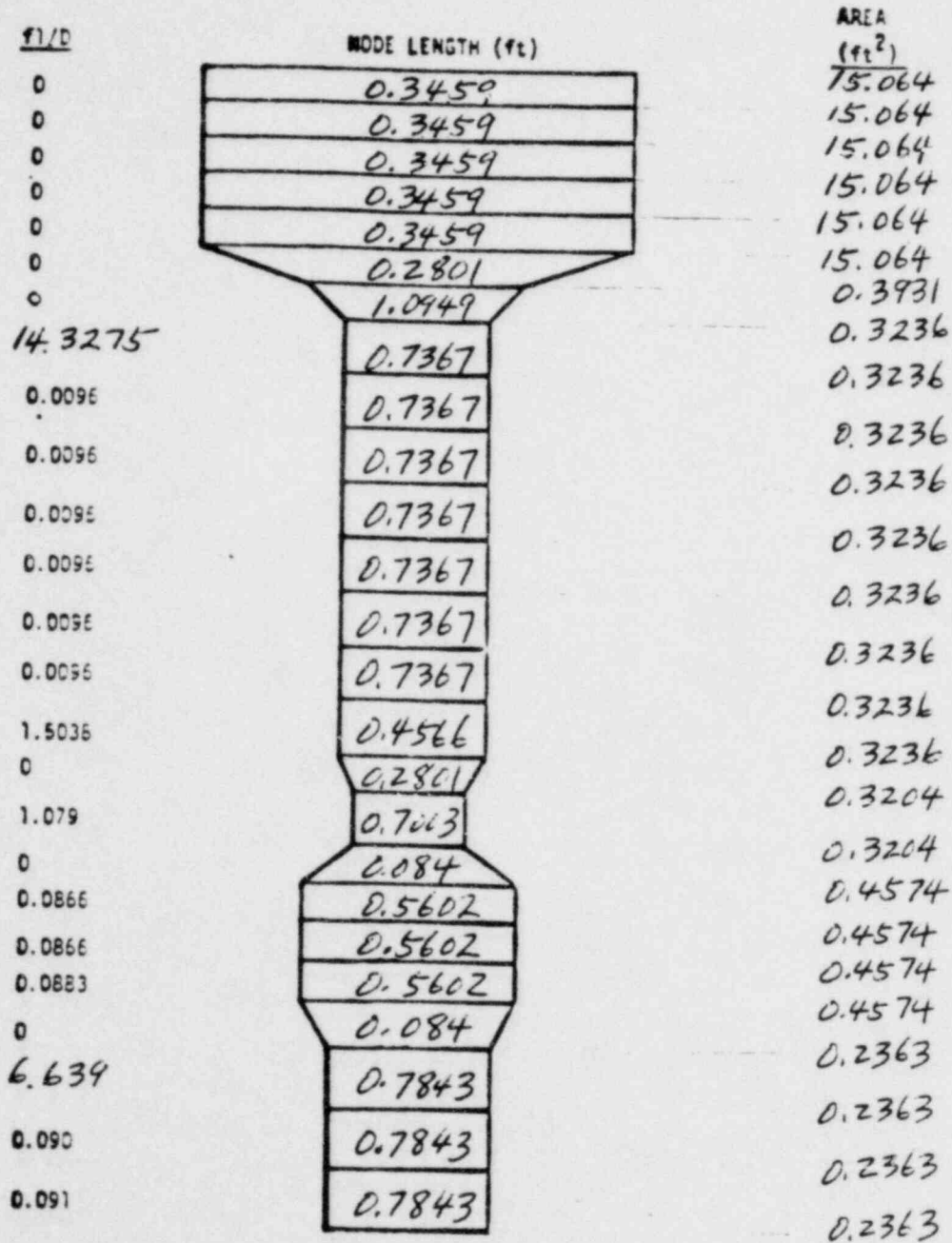


Figure 7A. Subscale Vent System with Majority of F1/D Lumped in Two Nodes

A124013

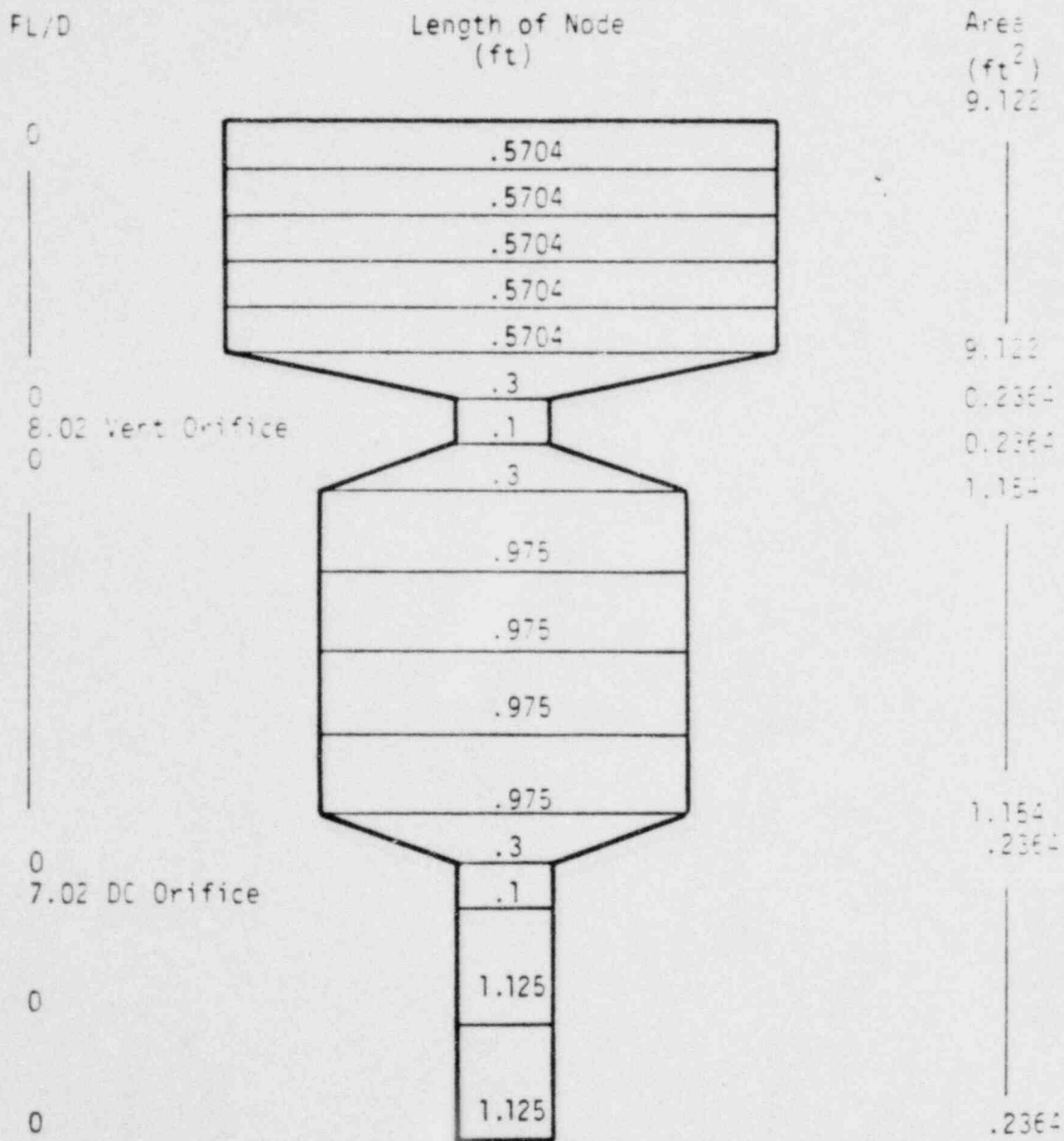


Figure 8. Nodal system -- QSTF "Perfect".

SYMBOL	SUBSCALE	FULL SCALE
P_{dw} (Psi/sec)	0	□
P_{exit} (Psi)	31.755	60
P_{inhal} (Psi)	4.2015	15
NORMALIZATION	4.2015	15
FI/D	FIGURE 7 DISTRIBUTED	FIGURE 6 DISTRIBUTED
Δt (SEC)	.00025	.0005

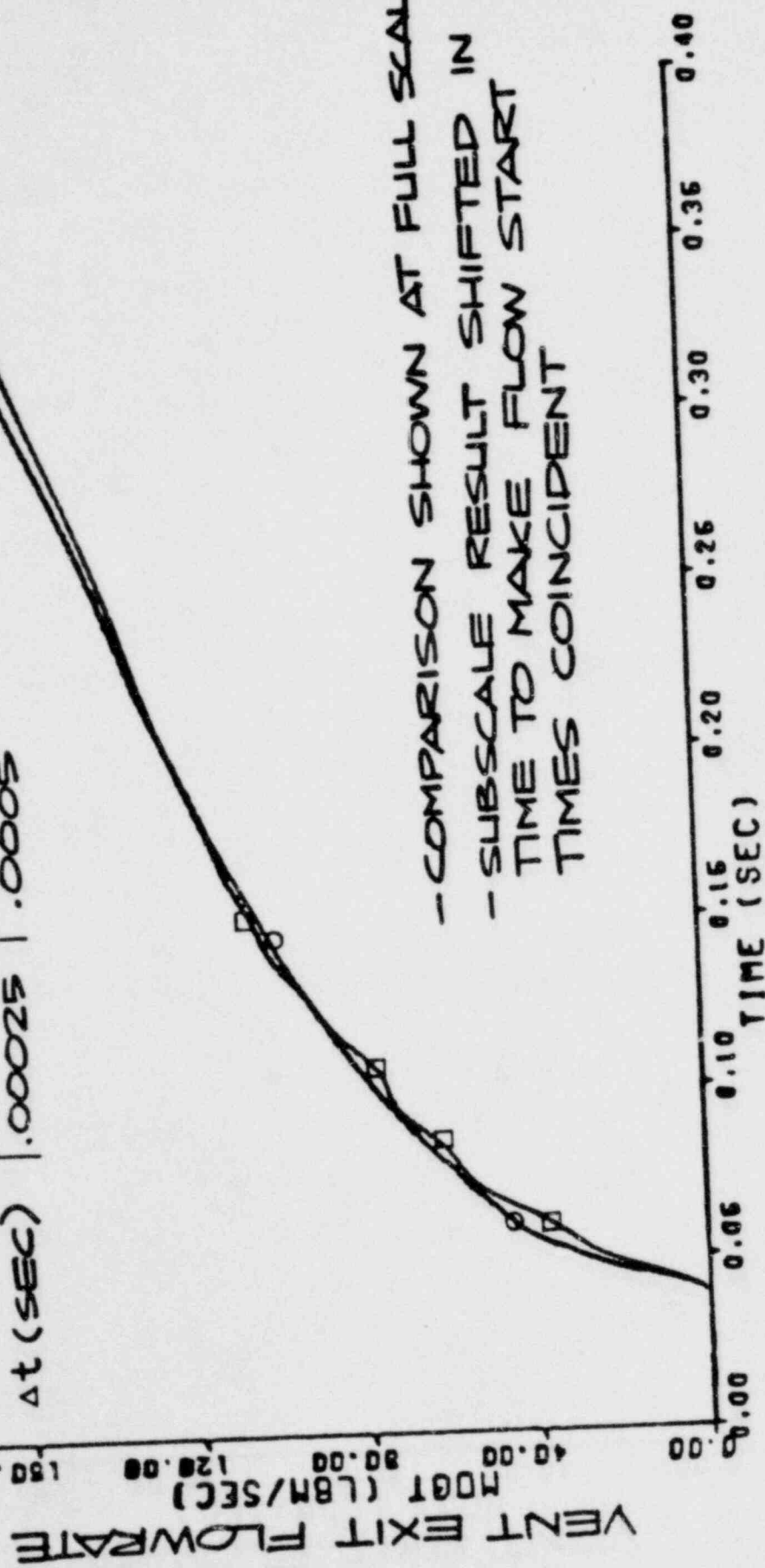


FIGURE 9. VENT EXIT FLOWRATE CASE 1 - CONSTANT P IN DRYWELL DISTRIBUTED LOSSES IN SUBSCALE

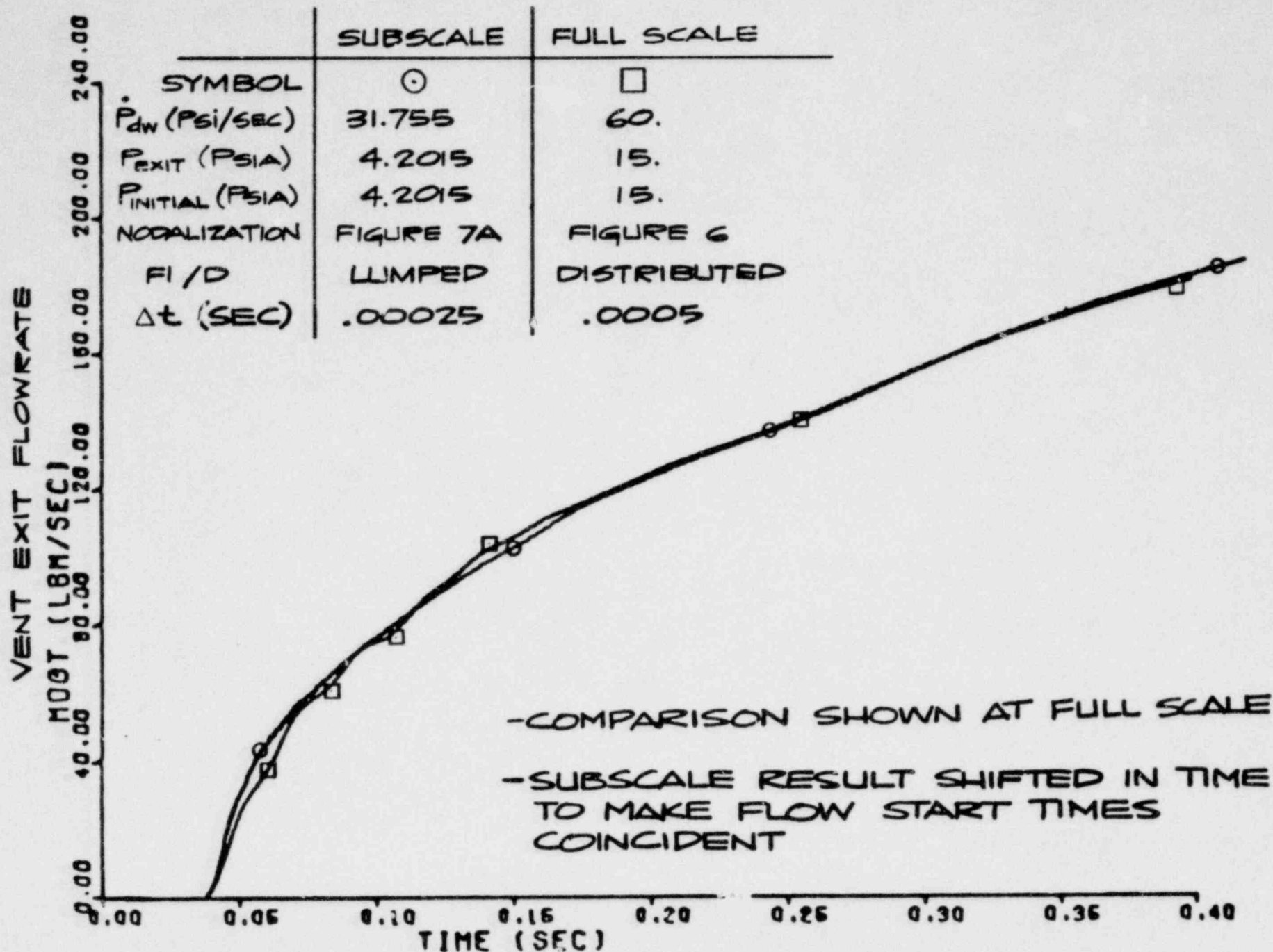


FIGURE 10. VENT EXIT FLOWRATE
CASE I - CONSTANT P IN DRYWELL
LUMPED LOSSES IN SUBSCALE

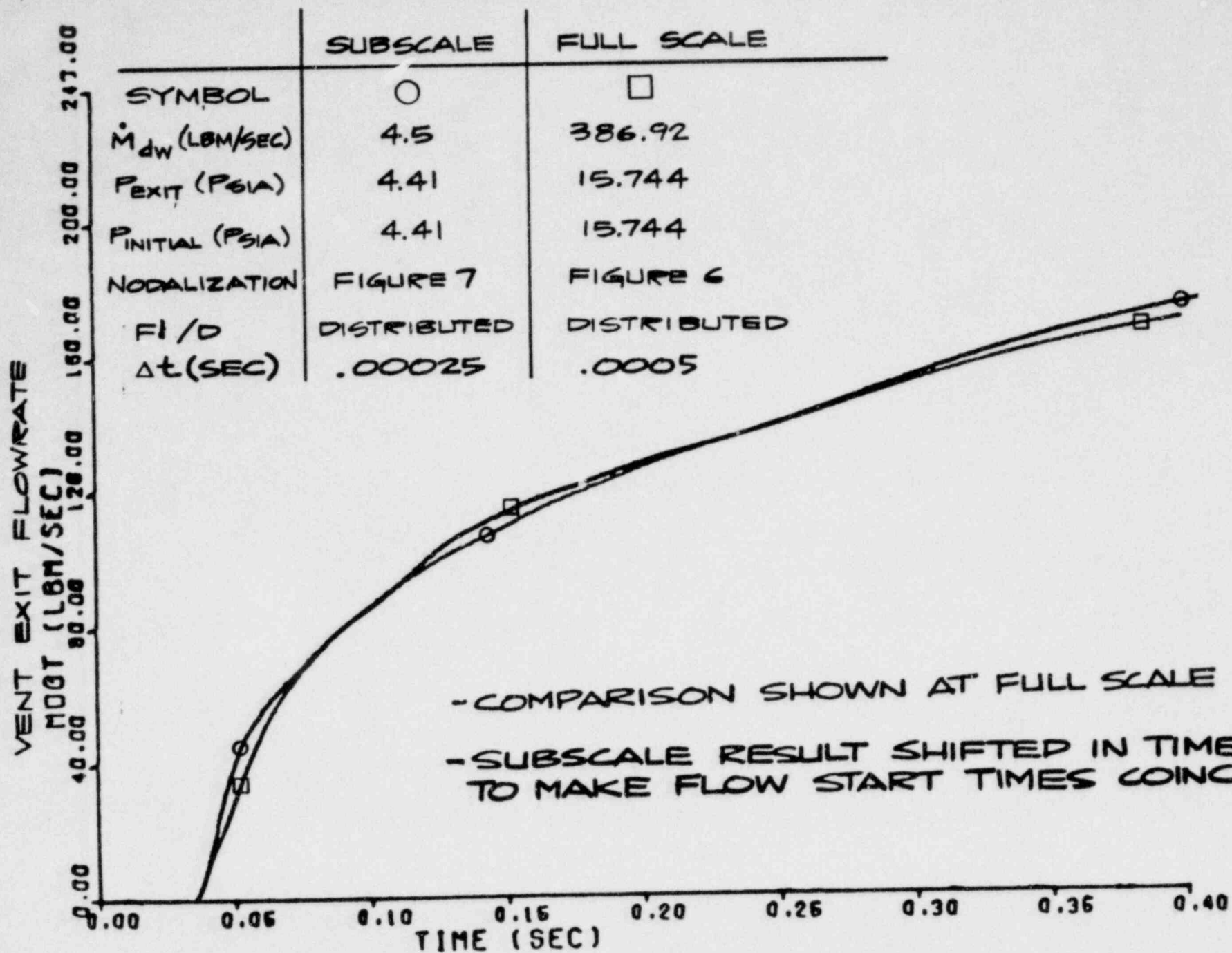


FIGURE II. VENT EXIT FLOWRATE
 CASE 3 - CONSTANT \dot{m} INTO DRYWELL
 DISTRIBUTED LOSSES IN SUBSCALE

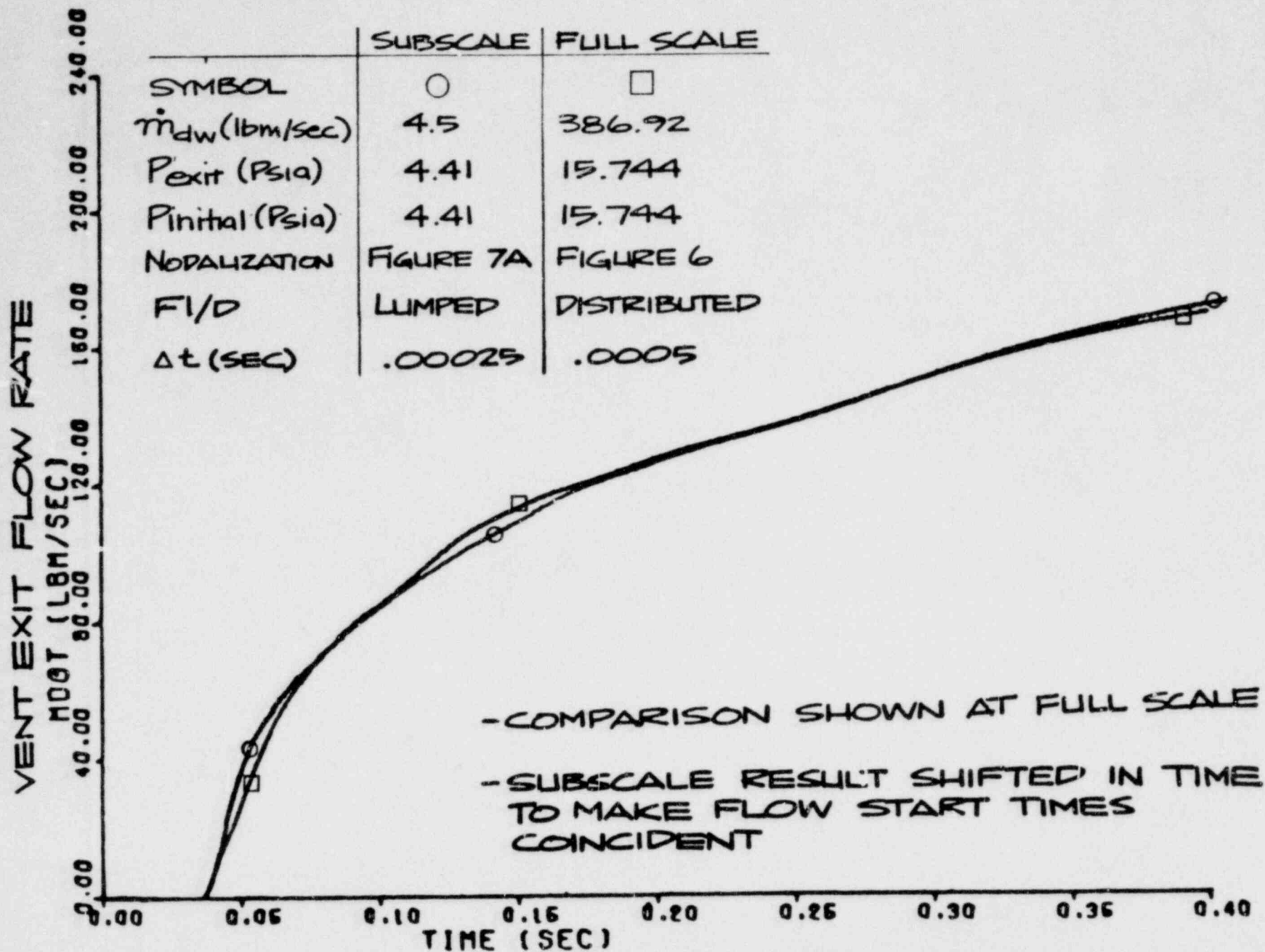
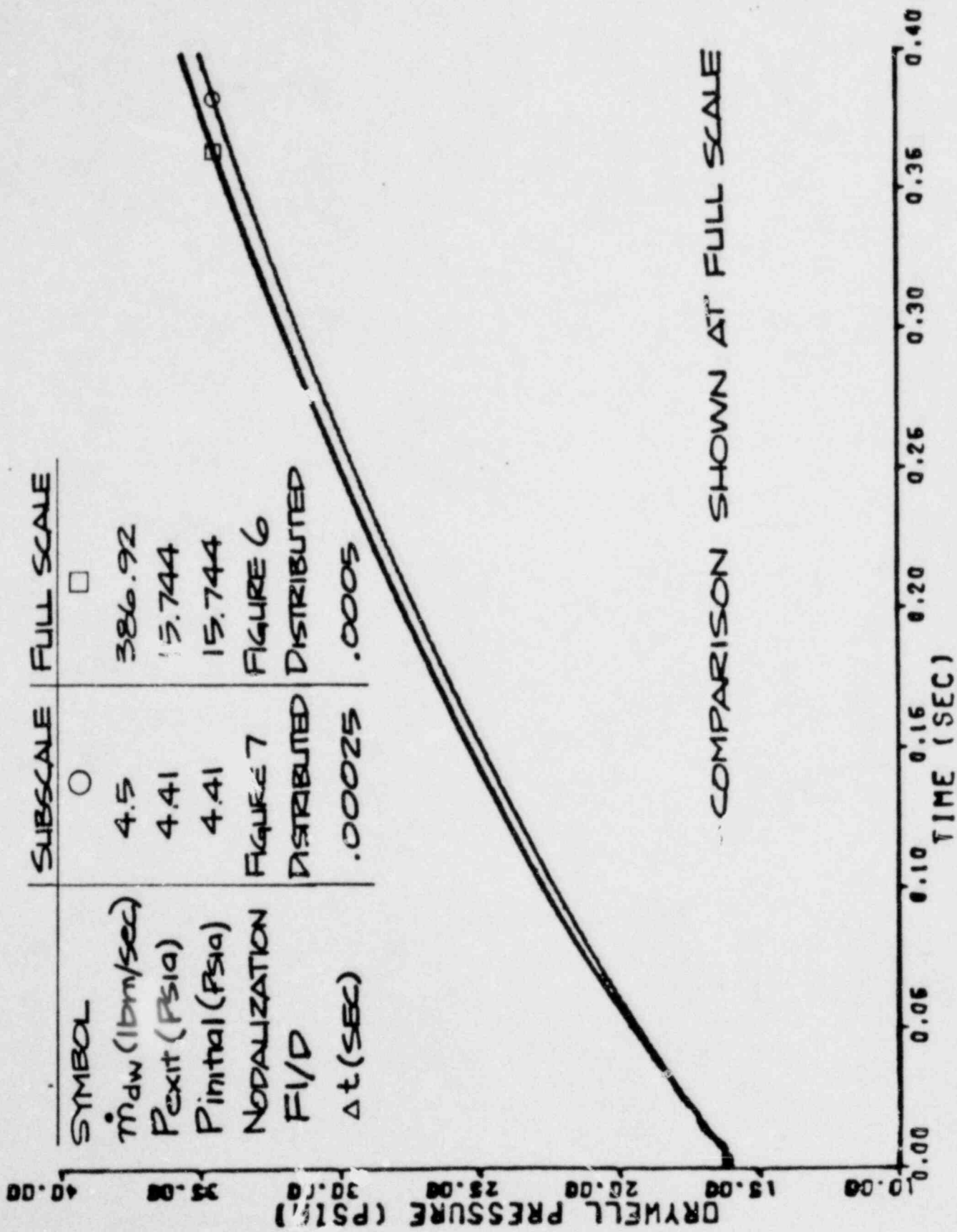


FIGURE 12. VENT EXIT FLOWRATE
CASE 3 - CONSTANT \dot{m} INTO DRYWELL
LUMPED LOSSES IN SUBSCALE



COMPARISON SHOWN AT FULL SCALE

FIGURE 13. DRYWELL PRESSURE CASE 3- CONSTANT \dot{m} INTO DRYWELL DISTRIBUTED LOSSES IN SUBSCALE

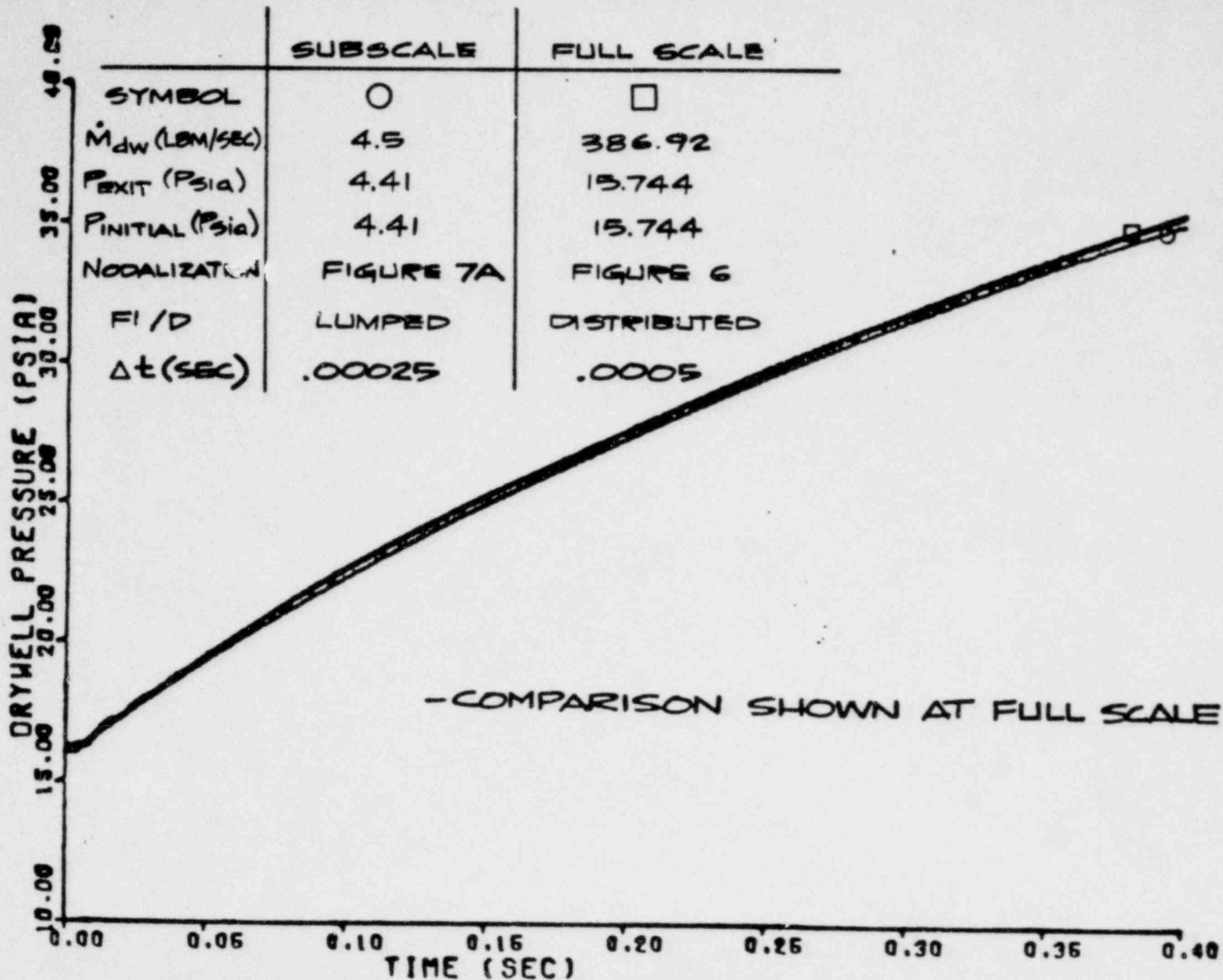


FIGURE 14. DRYWELL PRESSURE
CASE 3 - CONSTANT \dot{m} INTO DRYWELL
LUMPED LOSSES IN SUBSCALE

SYMBOL	SUBSCALE	FULL SCALE
P_{dw} (Psia)	0	□
P_{exit} (Psia)	5.602	20.
$P_{initial}$ (Psia)	4.2015	15.
NODALIZATION	5.602	20.
FI / D.	FIGURE 7	FIGURE 6
Δt (SEC)	DISTRIBUTED	DISTRIBUTED
	.00025	.0005

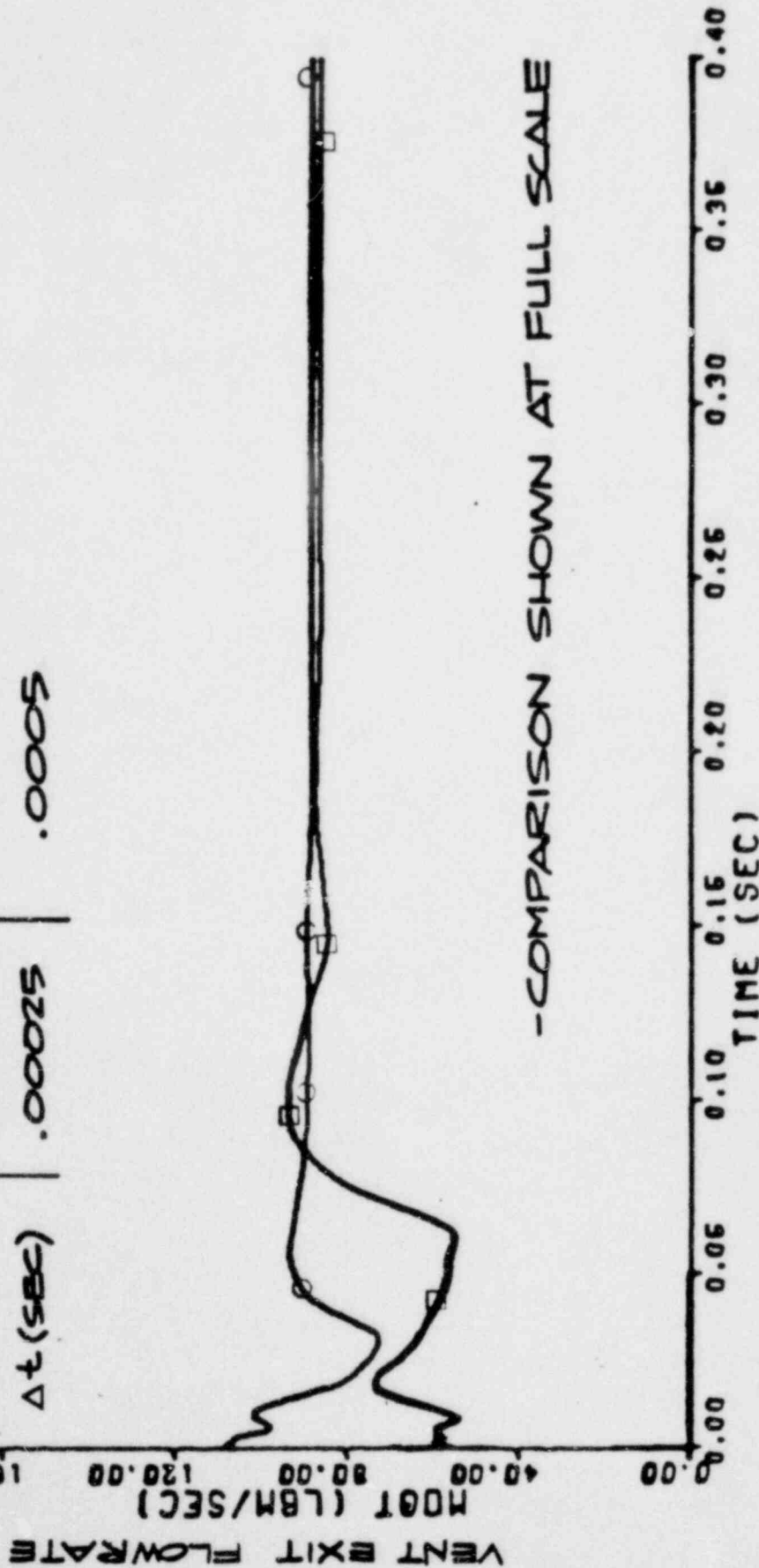
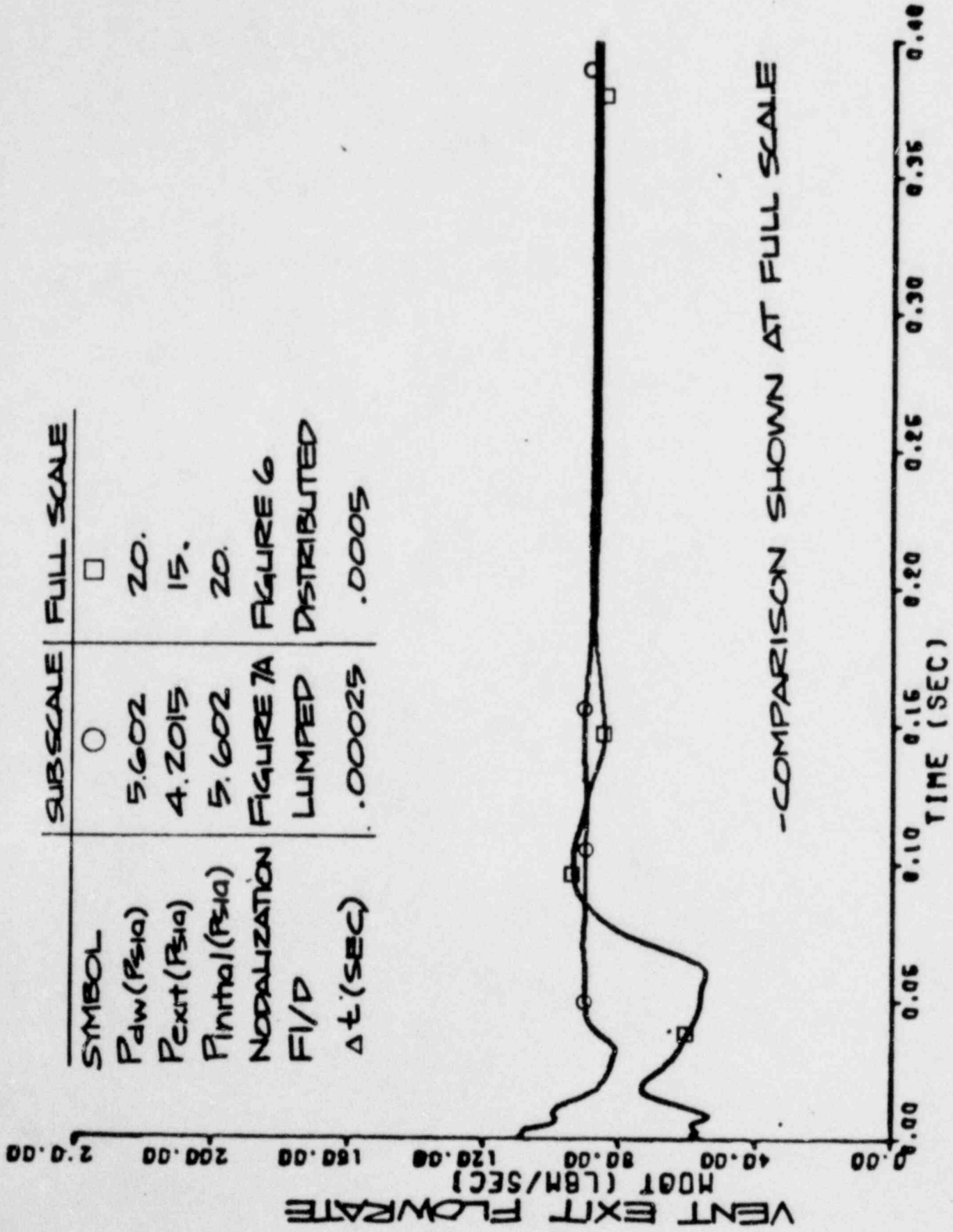


FIGURE 15. VENT EXIT FLOWRATE
CASE 2 - SUDDEN PRESSURE DROP AT EXIT
DISTRIBUTED LOSSES IN SUBSCALE



-COMPARISON SHOWN AT FULL SCALE

FIGURE 16. VENT EXIT FLOWRATE
CASE 2 - SUDDEN PRESSURE DROP AT
EXIT, LUMPED LOSSES IN SUBSCALE

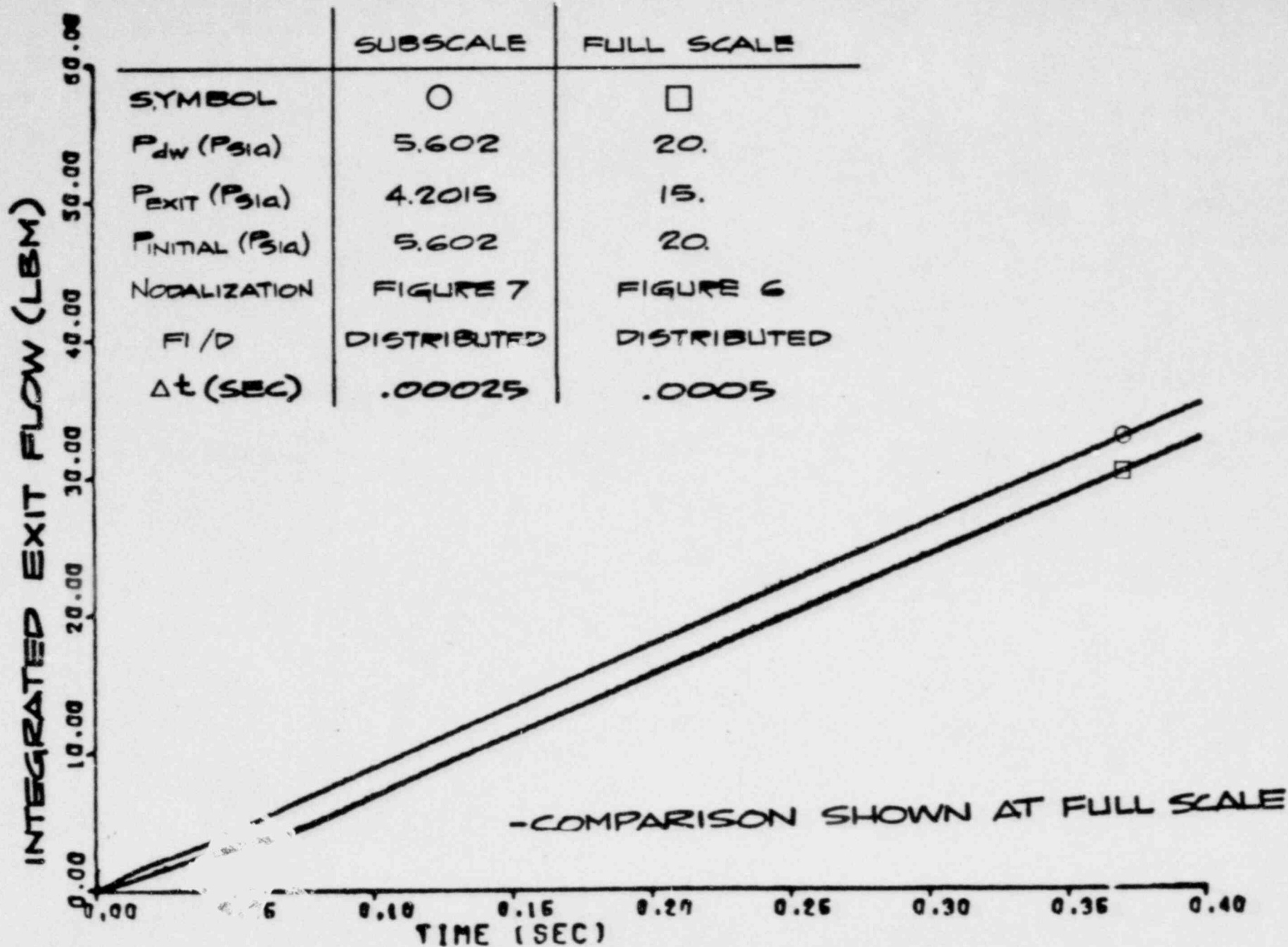


FIGURE 17. INTEGRATED MASS FLOW
CASE 2 - SUDDEN PRESSURE DROP AT
EXIT, DISTRIBUTED LOSSES IN SUBSCALE

SYMBOL	SUBSCALE	FULL SCALE
	○	□
P_{dw} (Psia)	5.602	20.
P_{exit} (Psia)	4.2015	15.
$P_{initial}$ (Psia)	5.602	20.
NORMALIZATION	FIGURE 7A	FIGURE 6
F/D	LUMPED	DISTRIBUTED
Δt (SEC)	.00025	.0005

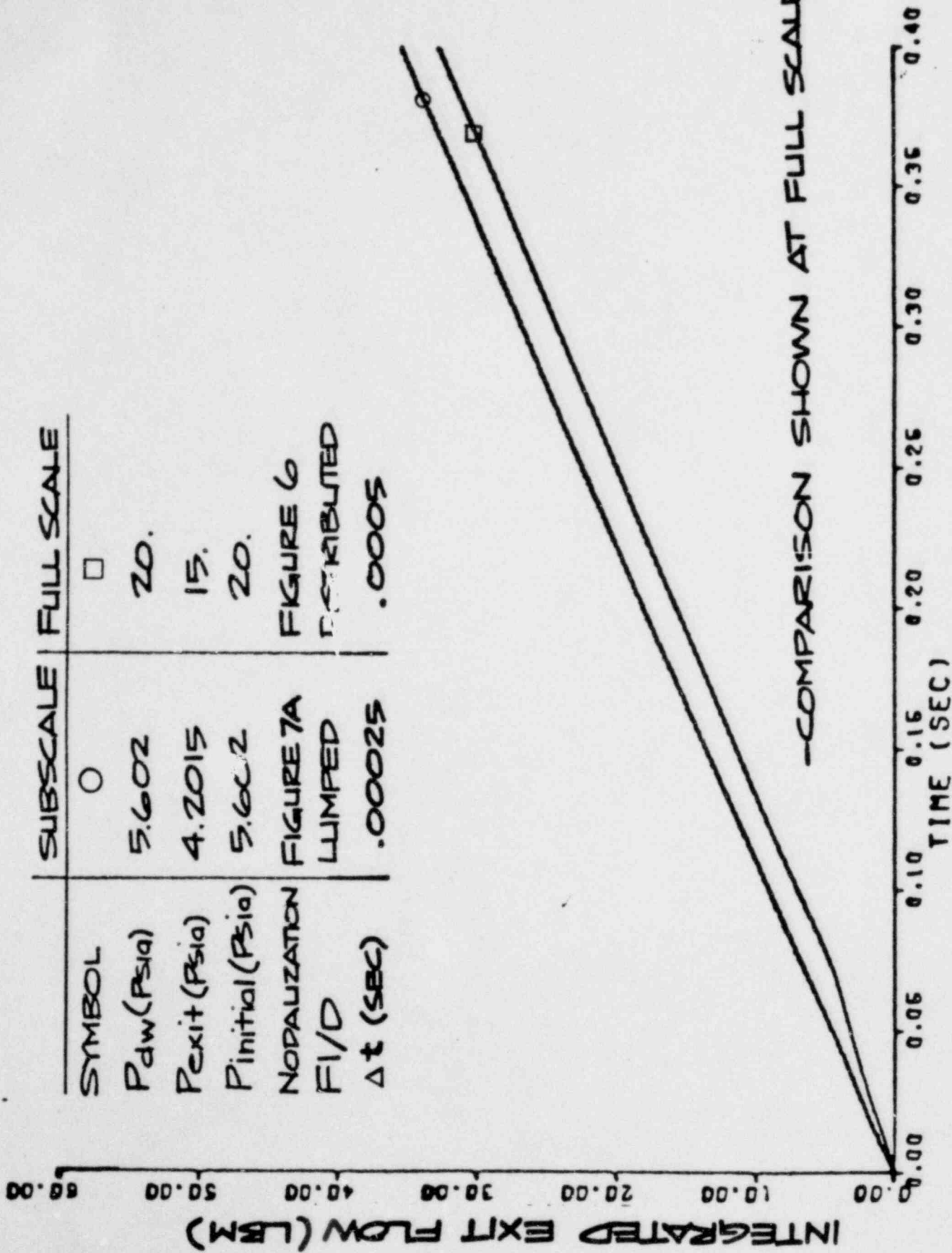
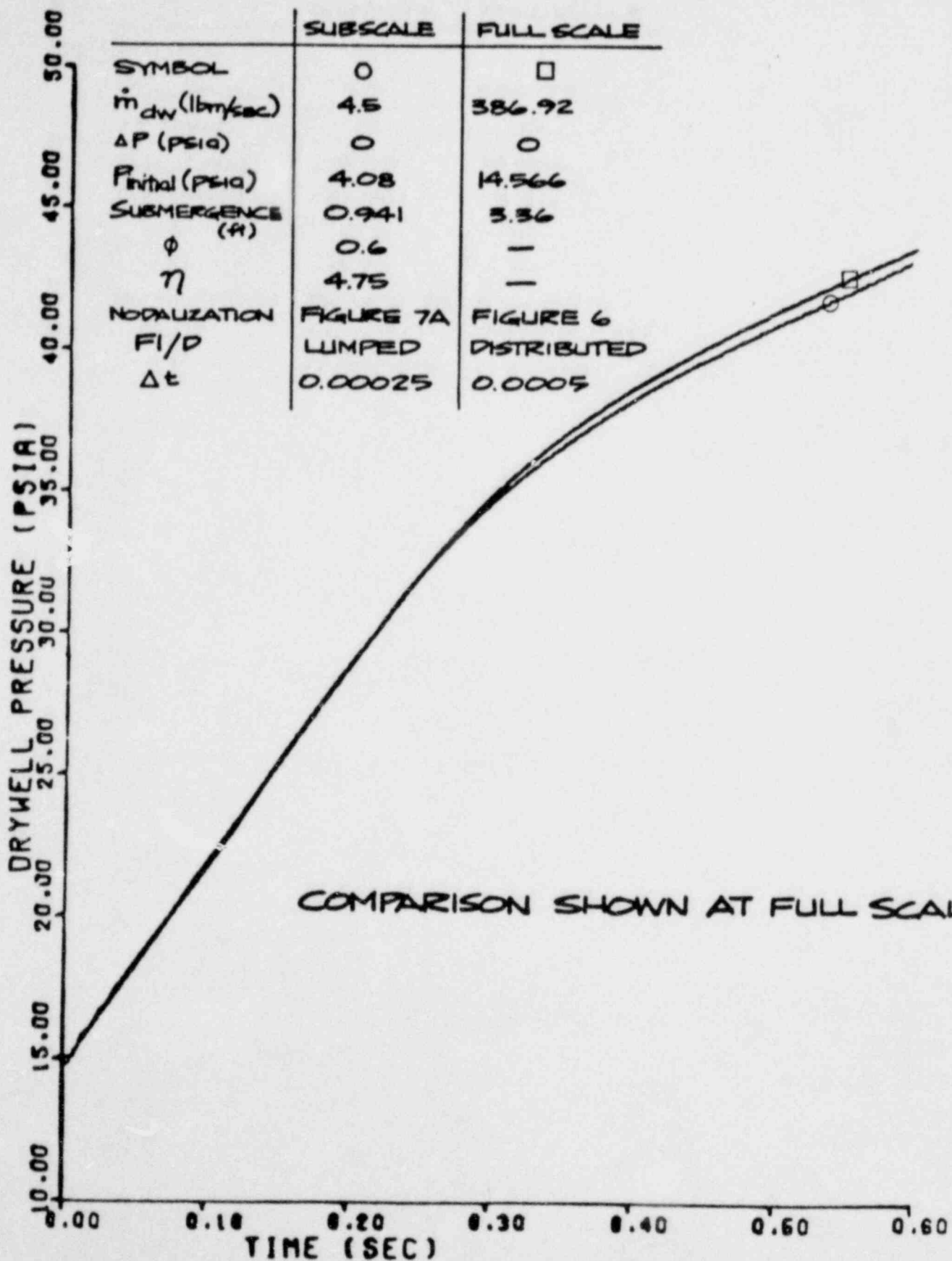


FIGURE 18. INTEGRATED MASS FLOW, CASE 2- SUDDEN PRESSURE DROP AT EXIT, LUMPED LOSSES IN SUBSCALE



COMPARISON SHOWN AT FULL SCALE

FIGURE 19. DRYWELL PRESSURE
CASE 4 - LUMPED MODEL IN SUBSCALE,
IMPOSED EXIT PRESSURE IN
FULL SCALE

	SUBSCALE	FULL SCALE
SYMBOL	0	□
\dot{m}_{dw} (lbm/sec)	4.5	386.92
ΔP (PSIA)	0	0
$P_{initial}$ (PSIA)	4.08	14.566
SUBMERGENCE (ft)	0.941	3.36
ϕ	0.6	—
η	4.75	—
NO DALUIZATION	FIGURE 7A	FIGURE 6
F1/D	LUMPED	DISTRIBUTED
Δt	0.00025	0.0005

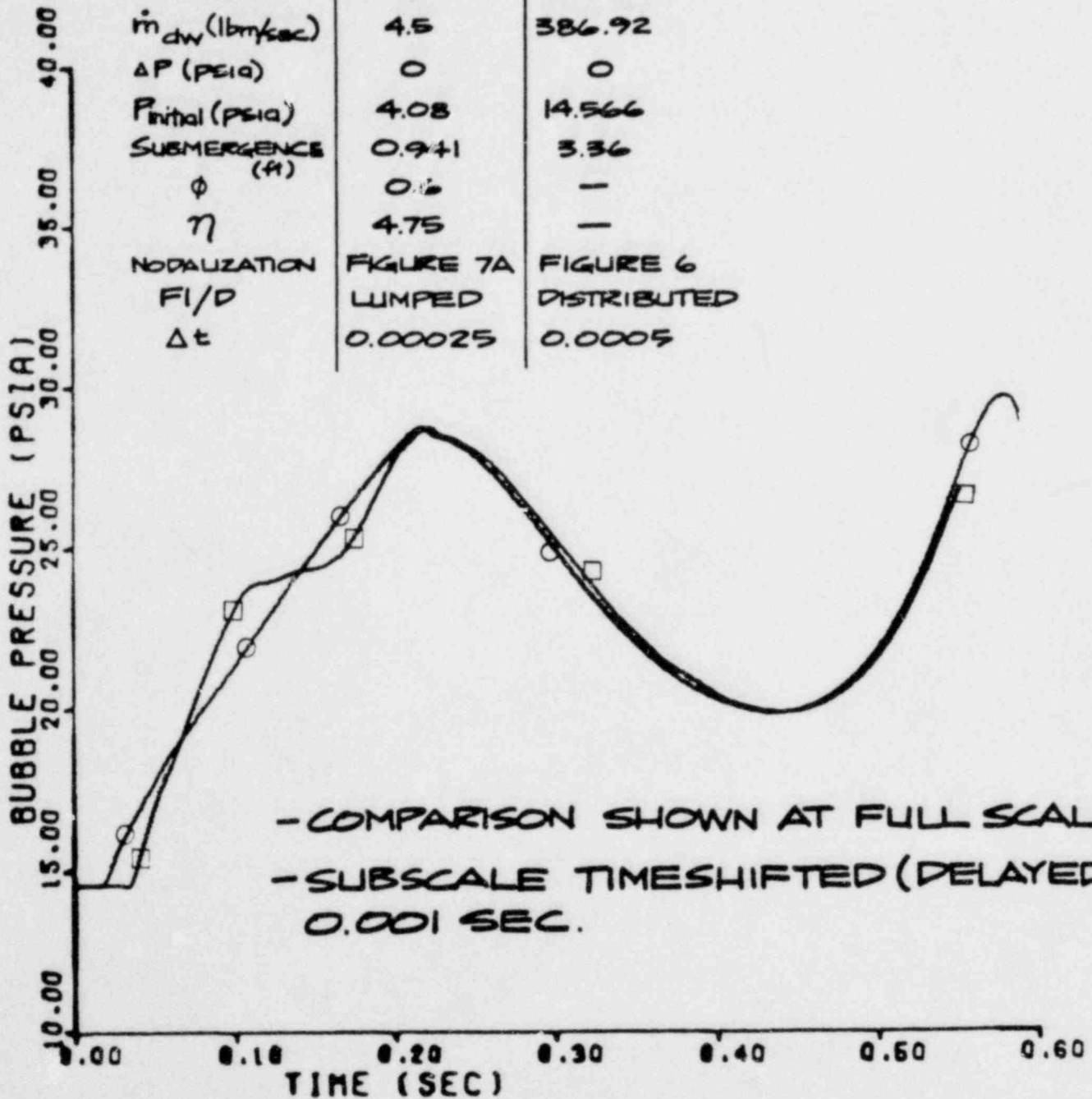


FIGURE 20. BUBBLE PRESSURE
CASE 4 - LUMPED MODEL IN SUBSCALE,
IMPOSED EXIT PRESSURE IN
FULL SCALE

	SUBSCALE	FULL SCALE
SYMBOL	○	□
\dot{m}_{dw} (lbm/sec)	4.5	386.92
ΔP (psia)	0	0
$P_{initial}$ (psia)	4.08	14.566
SUBMERGENCE ϕ (ft)	0.941	3.36
η	0.6	—
η	4.75	—
MODELIZATION	FIGURE 7A	FIGURE 6
F/D	LUMPED	DISTRIBUTED
Δt	0.00025	0.0005

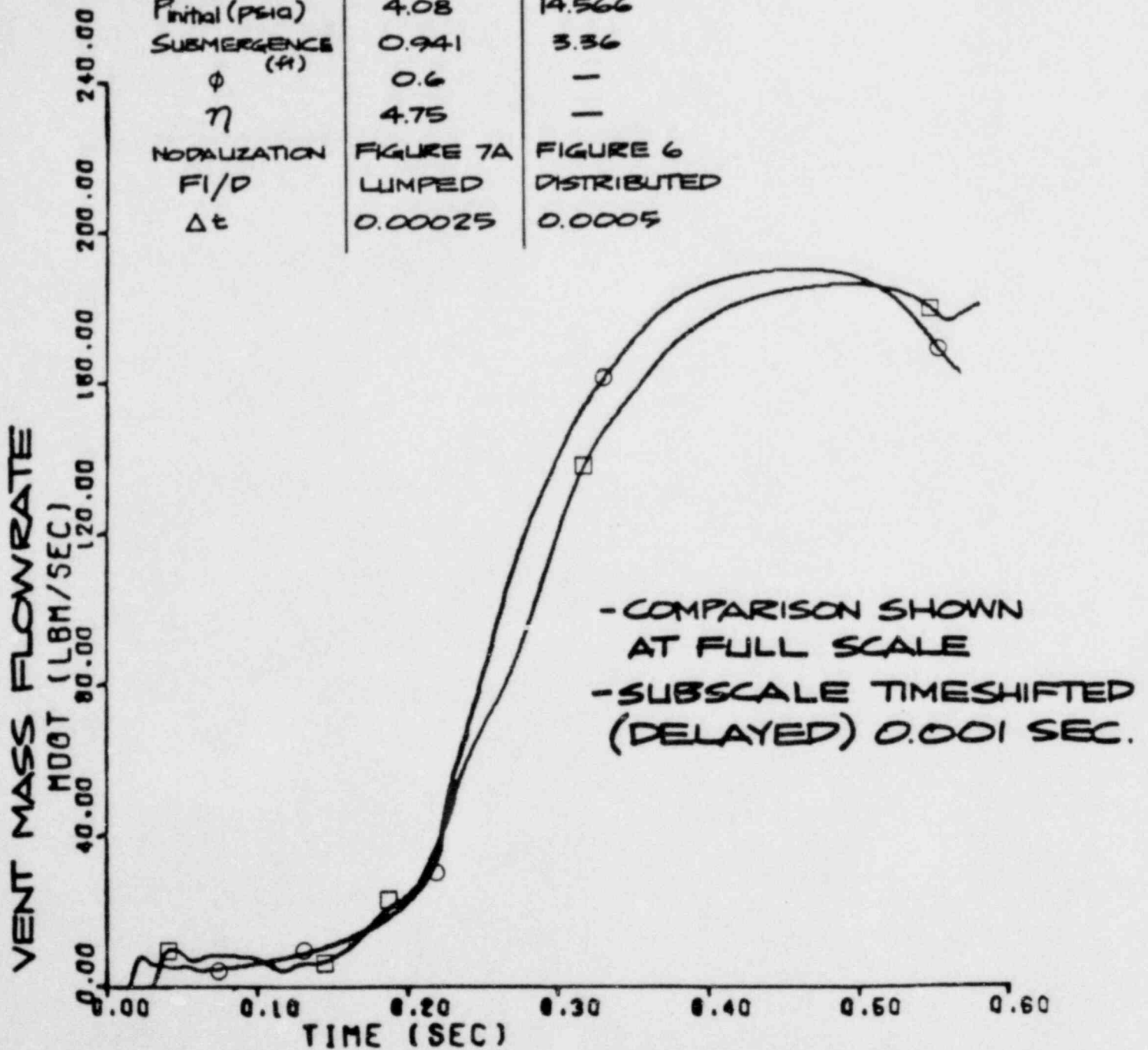


FIGURE 21. VENT MASS FLOWRATE
CASE 4 - LUMPED MODEL IN SUBSCALE,
IMPOSED EXIT PRESSURE IN
FULL SCALE

INTEGRATED VENT MASS FLOW (LBM)

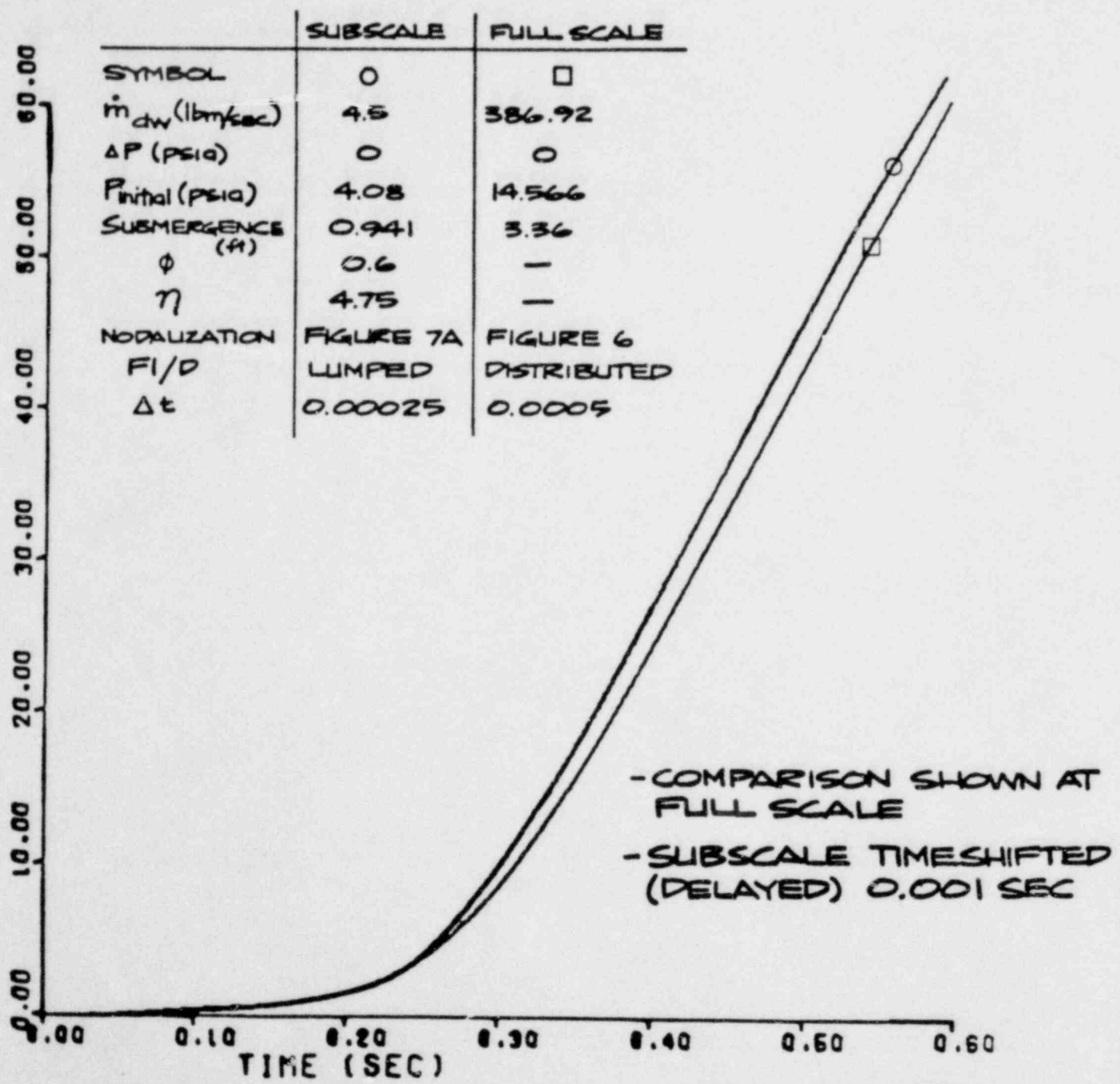


FIGURE 22. INTEGRATED VENT MASS FLOW CASE 4 - LUMPED MODEL IN SUBSCALE, IMPOSED EXIT PRESSURE IN FULL SCALE

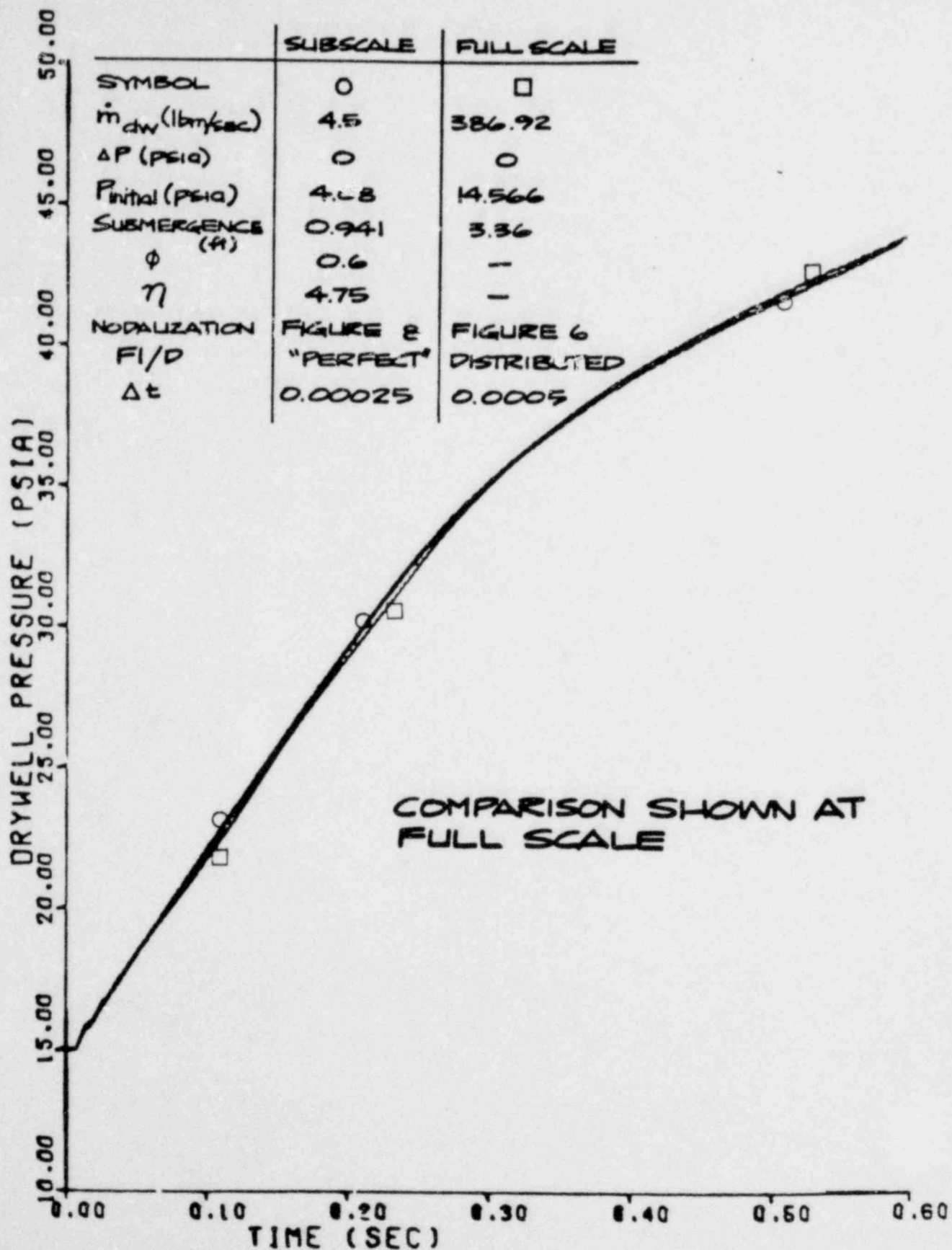


FIGURE 2.3. DRYWELL PRESSURE
 CASE 4A- QSTF "PERFECT" IN SUBSCALE
 IMPOSED EXIT PRESSURE IN
 FULL SCALE

	SUBSCALE	FULL SCALE
SYMBOL	○	□
\dot{m}_{dw} (lbm/sec)	4.5	386.92
ΔP (psia)	0	0
$P_{initial}$ (psia)	4.08	14.566
SUBMERGENCE (ft)	0.941	3.36
ϕ	0.6	-
η	4.75	-
NOZZLEIZATION	FIGURE 8	FIGURE 6
FI/D	"PERFECT"	DISTRIBUTED
Δt	0.00025	0.0005

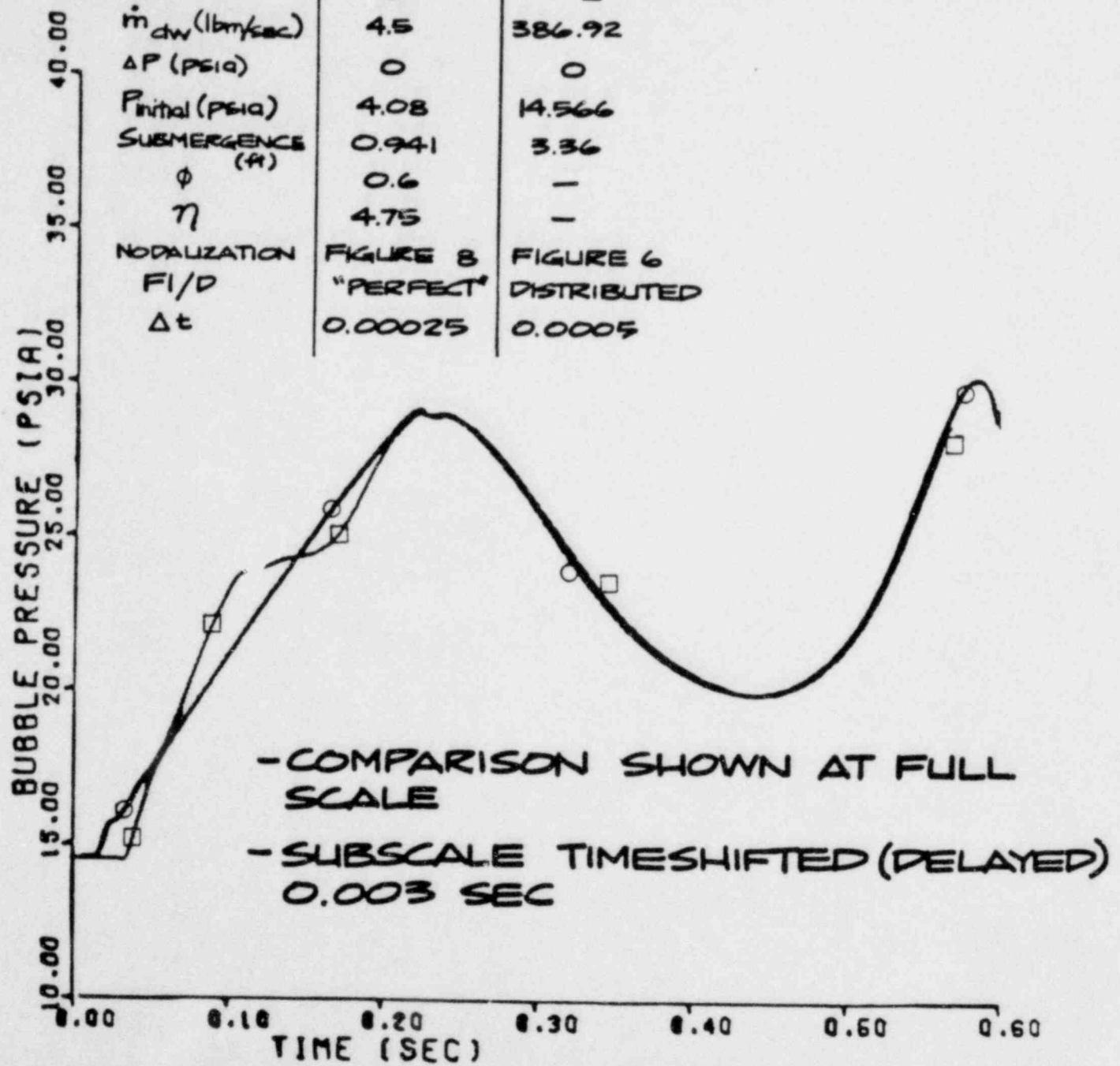


FIGURE 24. BUBBLE PRESSURE CASE 4A - QSTF "PERFECT" IN SUBSCALE IMPOSED EXIT PRESSURE IN FULL SCALE

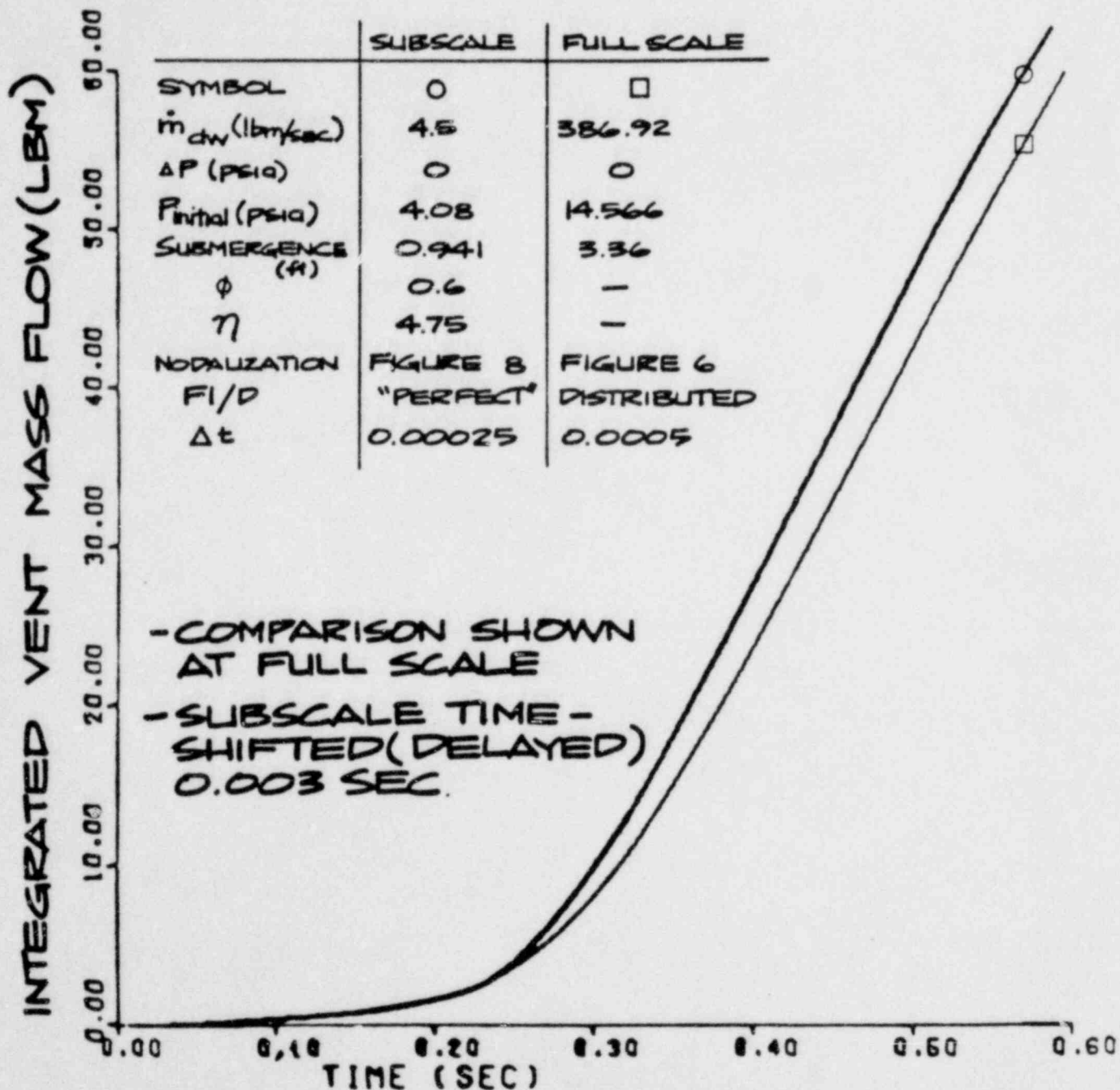


FIGURE 25. INTEGRATED VENT MASS FLOW CASE 4A - QSTF "PERFECT" IN SUBSCALE IMPOSED EXIT PRESSURE IN FULL SCALE

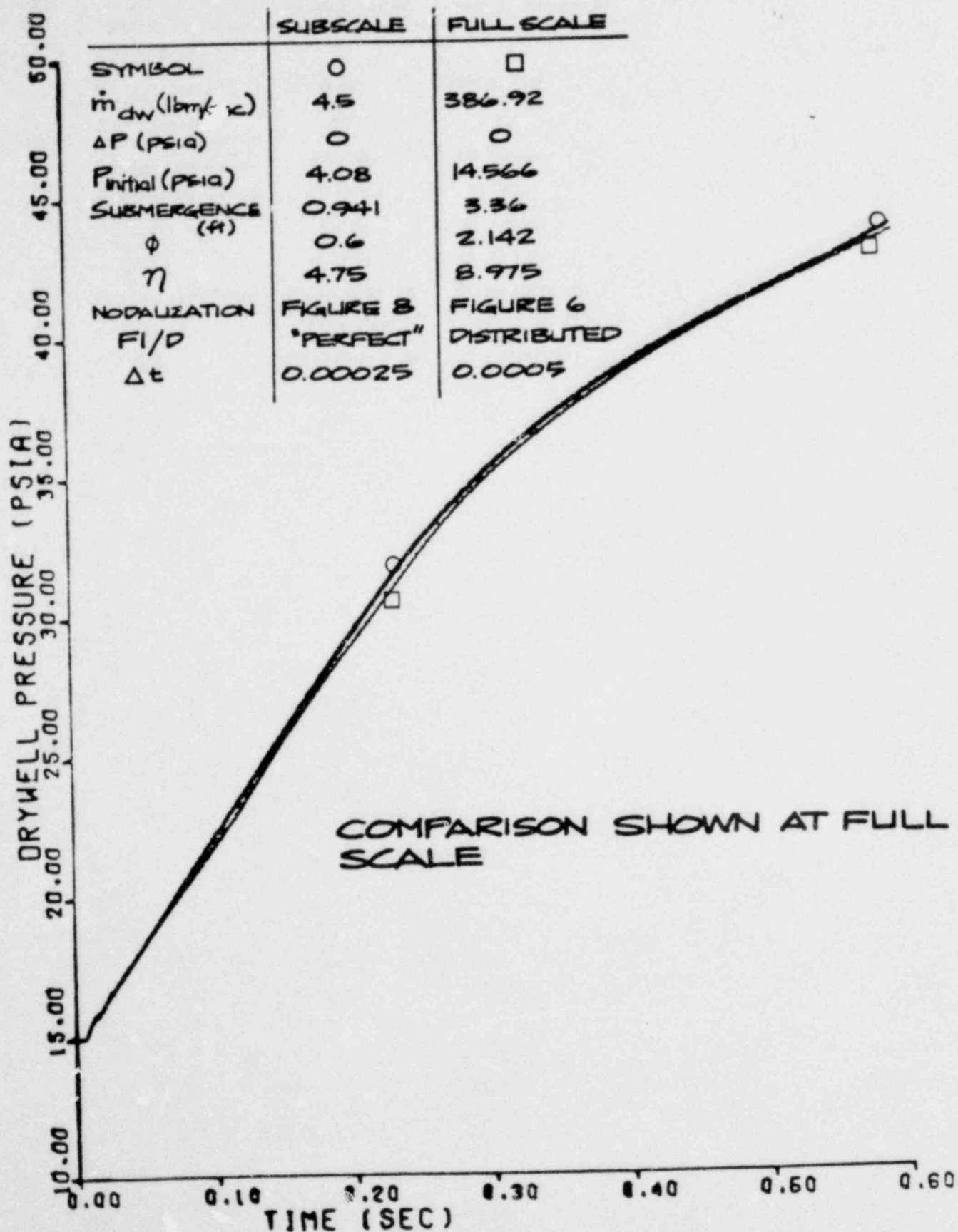


FIGURE 26. DRYWELL PRESSURE
CASE 5 - BUBBLE MODEL USED IN
SUBSCALE AND FULL SCALE

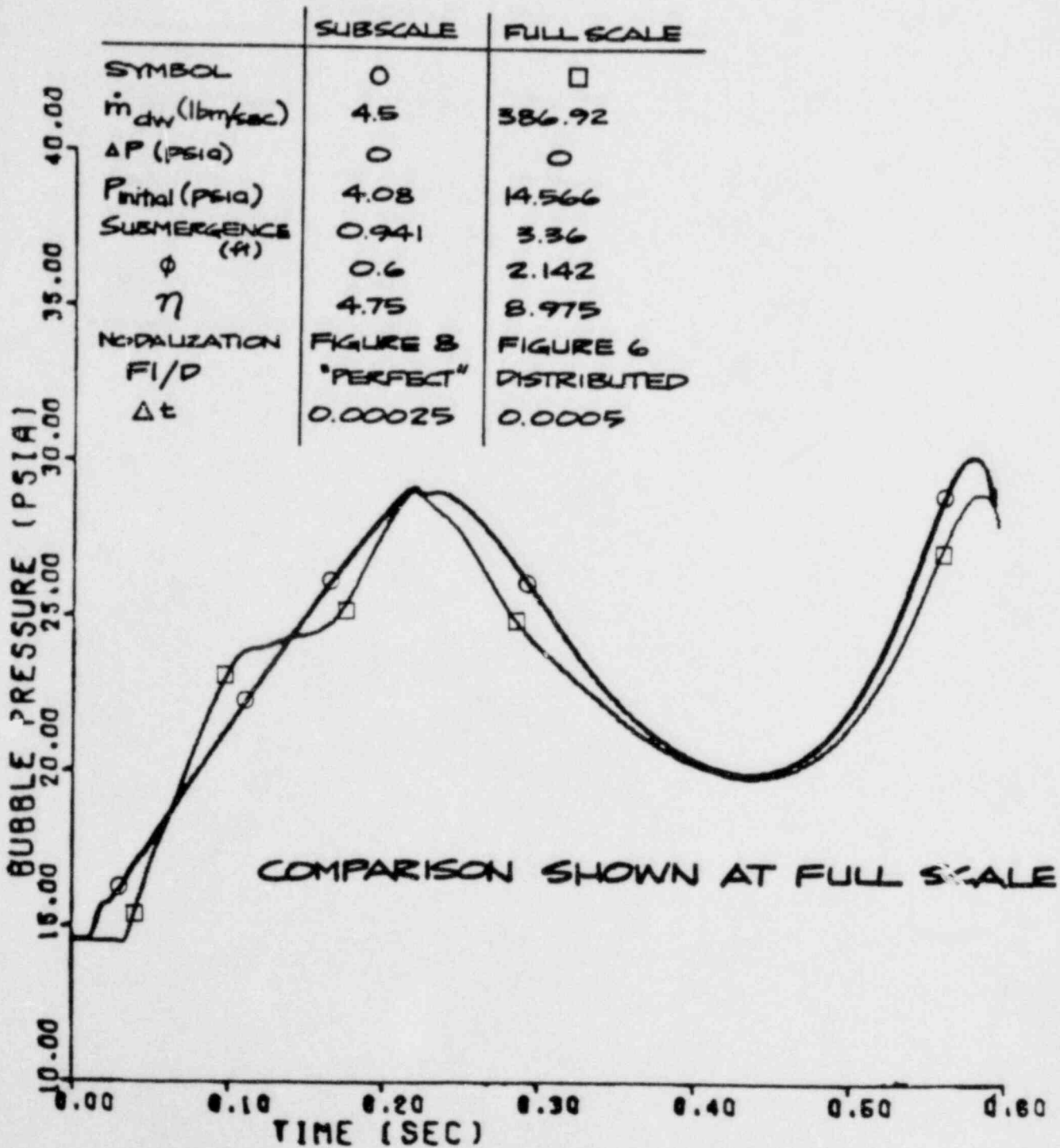


FIGURE 27. BUBBLE PRESSURE
CASE 5 - BUBBLE MODEL USED IN
SUBSCALE AND FULL SCALE

	SUBSCALE	FULL SCALE
SYMBOL	○	□
\dot{m}_{dw} (lbm/sec)	4.5	386.92
ΔP (psia)	0	0
$P_{initial}$ (psia)	4.08	14.566
SUBMERGENCE ϕ (#)	0.941	3.36
η	0.6	2.142
η	4.75	8.975
NOZZLEIZATION FI/D	FIGURE 8 "PERFECT"	FIGURE 6 DISTRIBUTED
Δt	0.00025	0.0005

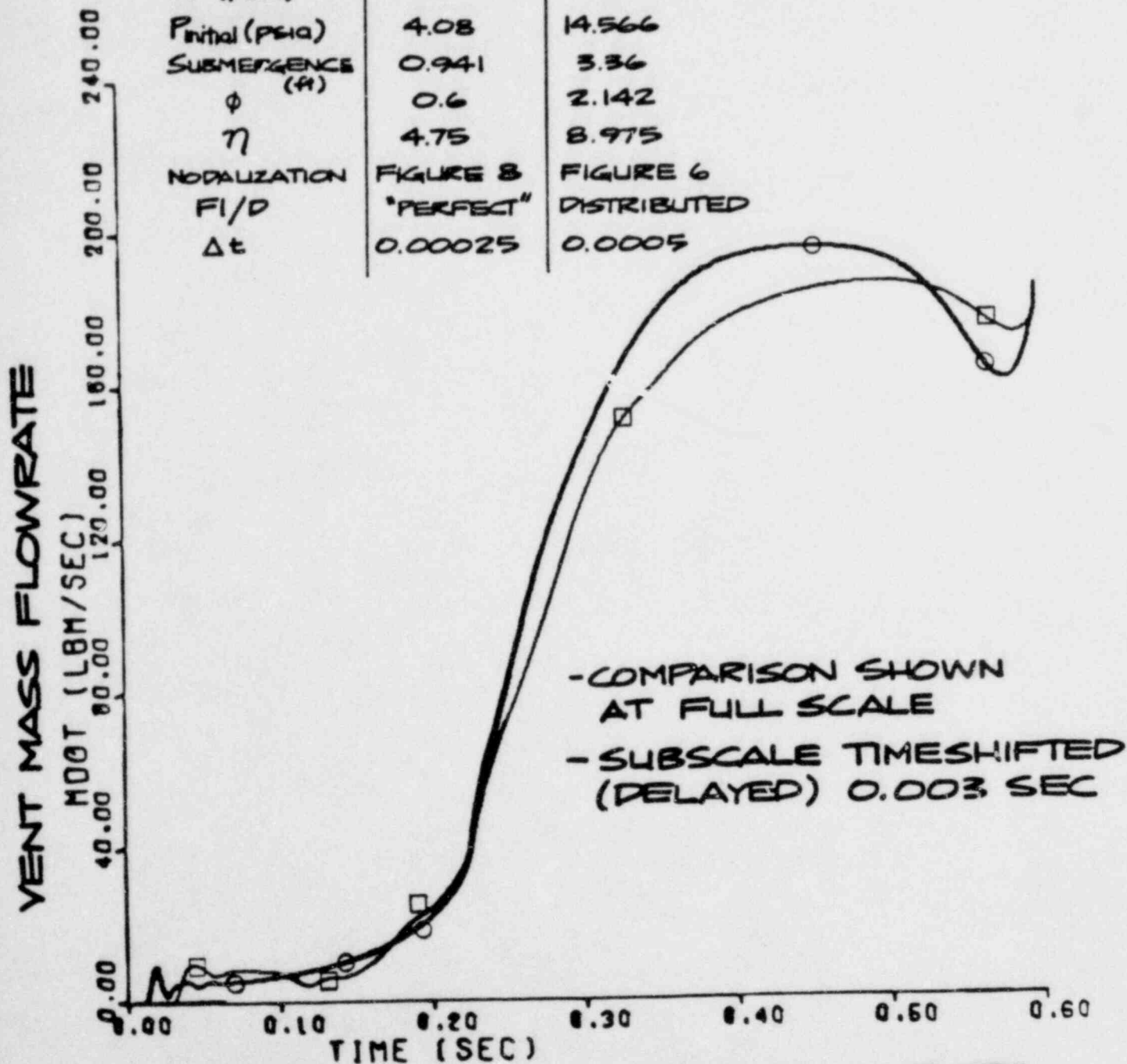


FIGURE 28. VENT MASS FLOWRATE
CASE 5 - BUBBLE MODEL USED
IN SUBSCALE AND FULLSCALE

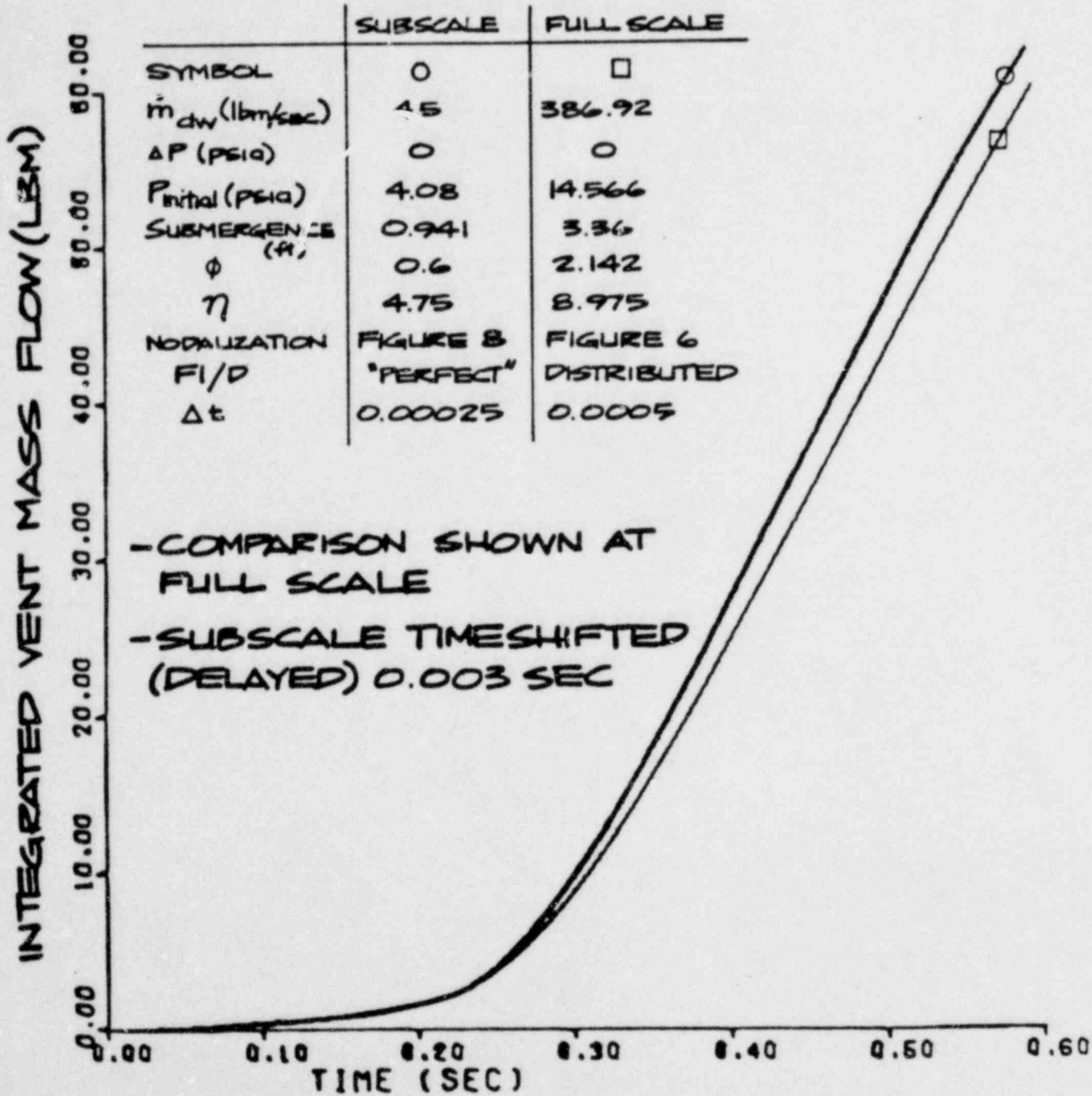


FIGURE 29. INTEGRATED VENT MASS FLOW
 CASE 5 - BUBBLE MODEL USED IN
 SUBSCALE AND FULLSCALE

APPENDIX A

EXIT VELOCITY SCALING IN STEADY, INCOMPRESSIBLE DUCT FLOW

Moody Scaling (Ref 2) from pool swell requires that vent exit velocity should be scaled as $\lambda^{1/2}$ where λ = scale factor, and pressure and density in the gas phase should be scaled as .

$$P_m = \lambda P_p \quad (1)$$

$$\rho_m = \lambda \rho_p \quad (2)$$

$$U_m = \lambda^{1/2} U_p \quad (3)$$

In the test cases the inlet stagnation pressure and exit static pressure of a duct system are specified. Moody scaling is to be applied such that the exit velocity in steady, incompressible flow is scaled according to equation (3). The stagnation pressure loss in steady constant area incompressible duct flow with friction is given by

$$P_{0i} - P_{0e} = K \frac{1}{2} \rho U^2 \quad (4)$$

where P_{0i} = entrance stagnation pressure

P_{0e} = exit stagnation pressure

K = loss coefficient (includes entrance, and internal duct losses but does not include dump loss)

ρ = density

U = duct velocity (equal everywhere in duct)

The incompressible Bernoulli equation:

$$P_{0e} = P_e + \frac{1}{2} \rho U^2 \quad (5)$$

Substituting equation (5) into (4) leads to

$$P_{0i} - P_e = (K+1) \left(\frac{1}{2} \rho U^2 \right) \quad (6)$$

applying equation (6) to model and prototype

(with subscripts M = model, P = prototype)

$$(K+1)_p = \frac{P_{oi_p} - P_{e_p}}{\frac{1}{2} \rho_p U_p^2} \quad (7)$$

$$(K+1)_m = \frac{P_{oi_m} - P_{e_m}}{\frac{1}{2} \rho_m U_m^2} \quad (8)$$

applying equations (1) (2) & (3) to (8) yields

$$(K+1)_m = \frac{1}{\lambda} \left(\frac{P_{oi_p} - P_{e_p}}{\frac{1}{2} \rho_p U_p^2} \right)$$

$$\text{OR } (K+1)_m = \frac{1}{\lambda} (K+1)_p \quad (9)$$

Thus scaling vent entrance stagnation and exit static pressures by λ and requiring that $U_e \sim \lambda^{1/2}$ leads to (9), i.e., the dump loss = 1.0 is added to the prototype duct loss coefficient before scaling and the sum scales to $(K+1)_M$.